



CZECH TECHNICAL UNIVERSITY IN PRAGUE

FACULTY OF BIOMEDICAL ENGINEERING

Department of Natural Sciences

Investigating mechanical properties of biopolymers

Výzkum mechanických vlastností biopolymerů

Master thesis

Study program: Biomedical and clinical technology
Study branch: Instruments and Methods for Biomedicine

Thesis supervisor: RNDr. Zdeněk Lánský, Ph.D.
Consultant: Ing. Vladimíra Petráková, Ph.D.

Bc. Anna Zelená

Kladno, June 2017

Academic year: 2016/2017

Diploma thesis assignment

(Master project thesis assignment)

Student: **Bc. Anna Zelená**
Study branch: Instruments and Methods for Biomedicine
Title: **Investigating mechanical properties of biopolymers**
Title in Czech: Výzkum mechanických vlastností biopolymerů

Instructions for processing:

- 1) Preparation of experiments with optical tweezer. Optimization of chemical and physical conditions for i) observation of single protein molecules with cytoskeletal fibres and DNA ii) manipulation with single cytoskeletal fibres and DNA molecules and iii) measuring of intermolecular forces.
- 2) Experimental characterizing of single molecule DNA elasticity.
- 3) Measuring of entropic forces produced by motor proteins kinesin-14 HSET.

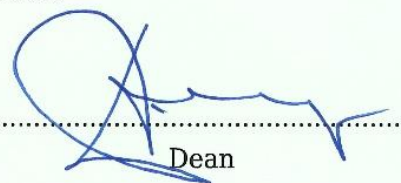
References:

- [1] Lansky Z, Braun M, Lüdecke A, Schlierf M, ten Wolde PR, Janson ME, Diez S, Diffusible crosslinkers generate directed forces in microtubule networks, Cell., Vol. 160, No. 6, 2015, 1159-68 s.
- [2] Moffitt, J.R. et al., Recent advances in optical tweezers, Annu. Rev. Biochem., Vol. 77, No. 205-228, 2008
- [3] Gross, P. et al., Revealing the competition between peeled ssDNA, melting bubbles, and S-DNA during DNA overstretching using fluorescence microscopy, Proc Natl Acad Sci USA, Vol. 10, No. 110, 2013, 3859-3864 s.

Validity of assignment until date: 20.08.2018
Supervisor of diploma thesis: RNDr. Zdeněk Lánský, Ph.D.
Consultant of diploma thesis: Ing. Vladimíra Petráková, Ph.D.



Head of Department



Dean

In Kladno, 24.02.2017

Katedra přírodovědných oborů

Akademický rok: 2016/2017

Z a d á n í d i p l o m o v é p r á c e

Student: **Bc. Anna Zelená**
Studijní obor: Přístroje a metody pro biomedicínu
Téma: **Výzkum mechanických vlastností biopolymerů**
Téma anglicky: Investigating mechanical properties of biopolymers

Z á s a d y p r o v y p r a c o v á n í :


- 1) Příprava pro experimenty s optickou pinzetou. Optimalizace chemických a fyzikálních podmínek pro i) sledování interakcí jednotlivých proteinových molekul s cytoskeletálními vlákny a DNA, ii) manipulaci s jednotlivými cytoskeletálními vlákny a molekulami DNA a iii) měření velikosti mezimolekulárních sil
- 2) Experimentální charakterizace elasticity jedné molekuly DNA
- 3) Měření entropických sil vytvářených motorovými proteiny kinesin-14 HSET

Seznam odborné literatury:

- [1] Lansky Z, Braun M, Lüdecke A, Schlierf M, ten Wolde PR, Janson ME, Diez S, Diffusible crosslinkers generate directed forces in microtubule networks, Cell., ročník 160, číslo 6, 2015, 1159-68 s.
- [2] Moffitt, J.R. et al., Recent advances in optical tweezers, Annu. Rev. Biochem., ročník 77, číslo 205-228, 2008
- [3] Gross, P. et al., Revealing the competition between peeled ssDNA, melting bubbles, and S-DNA during DNA overstretching using fluorescence microscopy, Proc Natl Acad Sci USA, ročník 10, číslo 110, 2013, 3859-3864 s.

Vedoucí: RNDr. Zdeněk Lánský, Ph.D.
Konzultant: Ing. Vladimíra Petráková, Ph.D.

Zadání platné do 20.08.2018


.....
vedoucí katedry / pracoviště


.....
děkan

V Kladně dne 05.01.2017

Prohlášení

Prohlašuji, že jsem diplomovou práci s názvem „Výzkum mechanických vlastností biopolymerů“ vypracovala samostatně a použila k tomu úplný výčet citací použitých pramenů, které uvádím v seznamu přiloženém k diplomové práci.

Nemám závažný důvod proti užití tohoto školního díla ve smyslu § 60 zákona č. 121/2000 Sb., o právu autorském, o právech souvisejících s právem autorským a o změně některých zákonů (autorský zákon).

V Kladně 19. 5.2017

.....
Bc. Anna Zelená

Acknowledgment

I would like to thank all the people who contributed in some way to the work described in this thesis. First and foremost, I thank my supervisor, Zdeněk Lánský, for giving me a great opportunity to work with modern microscopic methods and learn many new things, which I could not even imagine they exist. Every result described in this thesis was accomplished with the help and support of fellow labmates and collaborators, namely with Marcus Braun, Ondřej Kučera, Verena Henrichs, Silvie Svidenská and Ilia Zhernov. I would never have been able to finish my thesis without the guidance of my committee members and help from friends.

Název diplomové práce:

Výzkum mechanických vlastností biopolymerů

Abstrakt:

Buněčné pohyby jsou závislé na přeskupování vzájemně propojených biopolymerních sítí. Pro porozumění buněčným pohybům, jako je například buněčné dělení, je třeba nejdříve popsat mechanické vlastnosti biopolymerů zapojujících se do těchto procesů. Cílem této práce bylo popsat mechaniku dvou polymerních struktur: i) jednoho molekulárního vlákna DNA a ii) komplex mikrotubulů zesíťovaných molekulárním motorem kinesinem-14, HSET. Za tímto účelem jsme použili optickou pinzetu, umožňující přímou manipulaci a měření sil, v kombinaci se zobrazováním jednotlivých molekul pomocí fluorescenční mikroskopie.

Potvrdili jsme, že elastické chování jediné molekuly λ -DNA následuje model ohebného řetězce (worm-like chain) a k natažení molekuly (tzv. fáze overstretching) dochází okolo 65 pN. Zjistili jsme, že HSET váže mikrotubuly k sobě a vzájemně s nimi pohybuje a že tento pohyb zpomaluje, když se mikrotubuly začnou od sebe oddělovat. Ukázali jsme, že toto zastavení je způsobeno entropickou silou generovanou molekulami HSET, které jsou uzavřeny v překryvu mezi mikrotubuly. Změřili jsme tuto entropickou sílu a zjistili jsme, že je typicky v řádu pN, dosahující až ~ 20 pN. Naše výsledky představují nový pohled na fungování molekulárních motorů v kontextu biopolymerních sestav a budou použity k dalšímu popisu biopolymerních struktur s vyšší komplexitou.

Klíčová slova:

Optická pinzeta, lidský kinesin-14 HSET, TIRF mikroskopie, konfokální mikroskopie, mikrotubuly, motorové proteiny, DNA

Master's thesis title:

Investigating mechanical properties of biopolymers

Abstract:

Cellular movements depend on the rearrangement of the interconnected networks of biopolymers. To understand cellular movements like e.g. cell division we need to describe the mechanical properties of the biopolymers involved in these processes. The aim of this thesis was to describe the mechanics of two polymeric structures: i) a single DNA molecule and ii) a higher order assembly of microtubules crosslinked by kinesin-14, HSET, molecular motors. We used a combination of direct manipulation and force measurement by the optical tweezers with imaging of single molecules by fluorescence microscopy.

We confirmed that the elastic behaviour of a single λ -DNA molecule follows the worm-like chain model and that the molecule over-stretches at ~ 65 pN. We found that HSET crosslinks and slides microtubules and that this sliding stalls when the microtubules start to separate. We show that the stopping is due to an entropic force generated by HSET molecules confined in the overlap between the microtubules. We quantified the entropic force to be in the pN range, reaching up to ~ 20 pN. Our results represent a novel insight into the functioning of molecular motors in context of biopolymer assemblies and will be used to further describe the biopolymer structures of higher complexities.

Keywords:

Optical tweezers, human kinesin-14 HSET, total internal reflection microscopy (TIRF), confocal microscopy, microtubules, motor proteins, DNA

Content

Abbreviations.....	10
List of figures.....	11
1 Introduction.....	12
2 State of the Art.....	13
2.1 Biological Background.....	13
2.1.1 Microtubules	13
2.1.2 Motor proteins.....	14
2.1.3 Kinesin - 14.....	16
2.1.4 Elasticity of DNA	16
2.2 Technical Background	18
2.2.1 Optical tweezers.....	18
2.2.2 Microscopy techniques	26
3 Methods and materials	30
3.1 C-Trap optical tweezers	30
3.1.1 Microfluidic system	33
3.2 DNA experimental set up.....	34
3.2.1 DNA fluorescent probe	35
3.3 Kinesin – 14 HSET experimental set up	36
3.3.1 TIRF experimental set up	36
3.3.2 Optical tweezers experimental set up	37
3.3.3 Correlation of fluorescent imaging with force measurements.....	39
4 Results.....	40
4.1 DNA investigation results	40
4.1.1 DNA Elasticity.....	41
4.1.2 Binding of DNA intercalators.....	43
4.2 Kinesin – 14 HSET experiments.....	46

4.2.1	TIRF experiment results	46
4.2.1	Optical tweezers experiment results	51
5	Discussion.....	55
5.1	DNA Experiment	55
5.2	Kinesin – 14 HSET Experiments	56
5.2.1	TIRF microscopy experiment	56
5.2.2	Optical Tweezers force measurement.....	57
6	Conclusions.....	61
	List of Attachments.....	68

Abbreviations

ADP: adenosine diphosphate
ATP: adenosine triphosphate
BFP: back-focal plane
CMOS: complementary metal-oxide-semiconductor
DDS: dichlorodimethylsilane
dsDNA: double stranded DNA
GDP: guanosin diphosphat
GTP: guanosin triphosphat
GFP: green fluorescence protein
MB: motility buffer
MT: microtubule
MTOC: microtubule organize centre
NA: numerical aperture
nm: nanometer
OxSc: oxygen scavenger
PBS: phosphate buffered saline
PSD: position sensitive detector
QPD: quadrant photodiode detector
WLC: worm-like chain model
 μm : micrometer

List of figures

Figure 1: Structure of microtubule fibre	14
Figure 2: Types of motor proteins	15
Figure 3: Trapped beads in focused laser beam.....	21
Figure 4: Dielectric sphere displacement.....	22
Figure 5: Back-focal plane interference pattern	24
Figure 6: Power spectrum	26
Figure 7: Emission and excitation spectrums.....	29
Figure 8: Schematic diagram of the C-Trap device.....	31
Figure 9: Optical tweezer C-Trap	32
Figure 10: Inbuilt LabView software for optical tweezer.....	32
Figure 11: 4 channel laminar flow cell	33
Figure 12: Tethered molecule of dsDNA.	34
Figure 13: Layout of positions inside flow cell for DNA.....	35
Figure 14: Sample holder and microfluidic chamber.	37
Figure 15: Schema of flow cell with the assay for GFP-HSET experiment.....	38
Figure 16: Example of result for correlation of time	39
Figure 17: Force-distance curve of lambda DNA.....	42
Figure 18: Confocal image of dsDNA tethered between two beads.....	43
Figure 19: Gaussian distributions of fluorescent density.....	44
Figure 20: Kymographs of binding fluorescent dye Sytox Orange to DNA	45
Figure 21 Increasing density of motor proteins in shortening overlaps.	47
Figure 22 Schematic explanation of entropic force existence	48
Figure 23 Sliding of two microtubules crosslinked with kinesin-14 HSET with ATP. .	49
Figure 24 Return of two microtubules crosslinked with kinesin-14 HSET with ADP...	50
Figure 25: Image results from entropic force investigation.....	52
Figure 26: Resulting force curve recorded by stepping movement of one of the traps..	53
Figure 27: Force distance curve for previous result.	54
Figure 28: Cut out from force/time graph showing offset force.....	54
Figure 29: Particles of gas inside the cylindrical volume.....	57
Figure 30: Mechanical deformation of microtubule	58
Figure 31: Comparison of two trapped beads visualized in bright field.....	59

1 Introduction

Biopolymers, like microtubules or actin filaments, provide the intracellular framework supporting the structure of the cell and providing the movement of other biopolymers, as for example DNA, organelles and whole eukaryotic cells. Cellular movements depend on the adaptive rearrangement of the interconnected networks of these biopolymers. To understand cellular movements like cell division, cell migration or intracellular transport we need to describe the mechanical properties of the biopolymers involved in these processes.

Typical generators of intracellular movement are microtubule-based molecular motors. Microtubules are cytoskeletal fibres, responsible for the formation of the higher order structures in the cell, as e.g. the mitotic spindle and serve as a path for motor proteins. Motor proteins, such as the members of the kinesin family, are enzymes that can transform chemical energy into mechanical movement. Kinesin-14 motors are known to cross-link microtubules and slide antiparallel microtubules relative to each other [1]. The mechanical properties of higher order structures arising from kinesin-14-mediated crosslinking of microtubules are however not understood.

To probe the mechanical properties of biopolymers, optical tweezers method is widely used. Optical tweezers employs focussed laser beam to manipulate micro-objects, such as polystyrene or silica beads. When attached to a biopolymer, such a micro-bead can serve as a handle to manipulate the biopolymer and to measure the forces required for the biopolymer manipulation. In this work, we used a state of the art correlative approach, combining the direct manipulation and force measurement by the optical tweezers with imaging of single molecules by fluorescence microscopy. Such approach allows for probing of mechanical properties while simultaneously visualizing the probed sample with single molecule resolution and is thus capable of delivering unparalleled insight into the probed system.

The aim of this thesis was to describe the mechanics of two polymeric structures: i) Describe the mechanics of a single DNA molecule. Recapitulating the measurements of DNA elastic properties performed earlier [2] would in our case serve as proof of principle experiment showing that our force measurement device is well set up and calibrated. ii) Describe the mechanics of a higher order assembly of microtubules crosslinked by human kinesin-14, HSET, molecular motors.

2 State of the Art

This chapter is divided into two parts. The first part introduces a biological background of my work (chapter 2.1) and contains a basic introduction to cytoskeletal structures and DNA. The second part describes a technical background of the thesis (chapter 2.2), such as optical tweezers and microscopy techniques important for my research.

2.1 Biological Background

2.1.1 Microtubules

Microtubules (MTs) are dynamic cytoskeletal fibres present in all eukaryotic cells that are involved in many internal cellular activities, including the cell division or an intracellular trafficking and give a shape to the whole cells. Their name is based on their tubular shape. They can grow up to 50 μm with inner diameter 17 nm and outer diameter 25 nm (Figure 1). They consist of 13 protofilaments and the monomer mass is approximately 55 kilodaltons. [3]

MTs are built from protein heterodimers known as α and β tubulin, which are oriented head to tail. Microtubules are, the same as their subunits, polarized – their minus end can be anchored in the nucleating complex in nucleation sites. In animal cells, they typically grow out of microtubule organize centre (MTOC), known as the centrosome with the plus-end-directed from the centre. MTs are dynamically unstable polymers, they continuously change their shape [4].

Microtubules switch between periods of growth and rapid shrinkage, that is referred to as dynamic instability. It can be described by 4 parameters: rate of growth, rate of shrinkage, frequency of switching from growth to shrinkage (catastrophe frequency) and frequency of switching from shrinkage back to growth (rescue frequency).

For *in vitro* experiments microtubules are polymerized from purified tubulin. The first step of the process of polymerization requires purified tubulin with the presence of Mg^{+2} ions and GTP in 37°C. This process, known as nucleation, requires some time for formation of the whole microtubule seed, during which, at first, the α and β tubulins are connected into dimers and lately attached to each other into protofilaments. Every addition of tubulins together requires energy provided by the hydrolysis of GTP into

GDP. The second part of the process is known as an elongation, during which short seeds of microtubules are connected and make microtubules longer into micrometre range. [5]

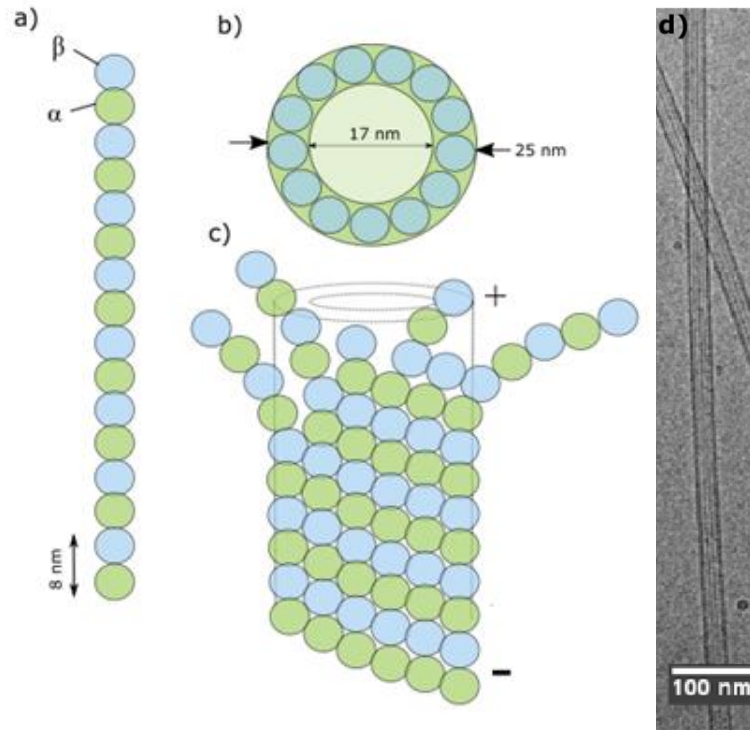


Figure 1: Structure of microtubule fibre

Schematic picture of a protofilament (a) and the whole microtubule structure (c) composed of tubulin heterodimers. Panel (b) shows the cross-section of microtubule with 13 protofilaments. (d) Transmission electron microscopy (TEM) image of GMPCPP double stabilized microtubules.

2.1.2 Motor proteins

Motor proteins are specific kind of proteins occurring inside living cells that are associated with the cytoskeleton. As their name suggests, they bind to cytoskeletal fibres and convert chemical energy in form of ATP into mechanical movement along cytoskeletal structure. Several families of them exist in eukaryotic cells and they can be divided according to their function, structure, or the fibre, which they use as a path for their movement. Many of motor proteins can transport a cargo along the filament structure in a cell or crosslink more fibres together and slide them against each other. [4]

Figure 2 shows three different family types of cytoskeletal motor proteins (myosin, kinesin and dynein). They use two types of cytoskeletal fibres as a path for their movement. Myosin interacts with actin filaments, while the kinesin and the dynein families are microtubule-associated motors. [6]

Kinesins are typically composed of a glomerular motor domain, also referred to as a head. It contains a site for ATP hydrolysis and a nucleotide-dependent binding site to the track. Each ATP hydrolysis event provides energy for one step, which is about 8 nm long, which corresponds to the length of one tubulin heterodimer. According to the type of the motor protein, they move in direction of the plus or minus-end of the microtubule. [6]

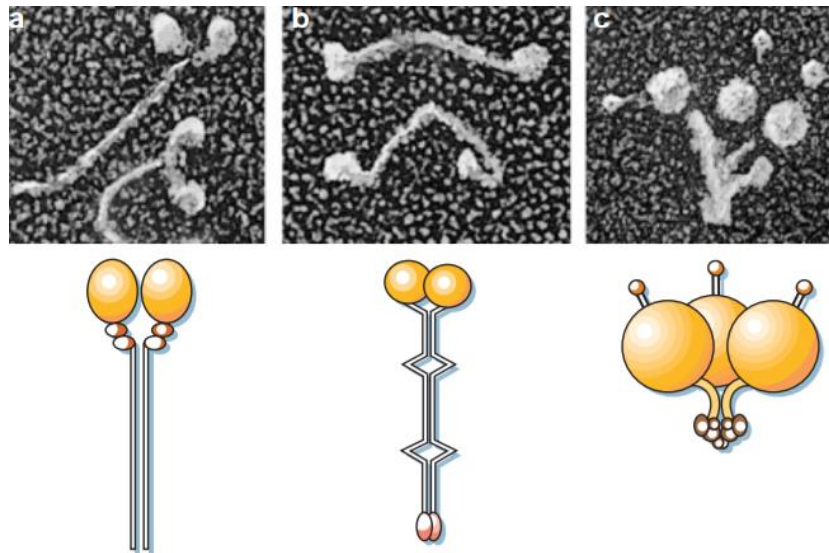


Figure 2: Types of motor proteins

From left: myosin II (a), kinesin (b) and ciliary dynein (c). In the top row are images from transmission electron microscopy, schematic structure depicted below. Catalytic site of heavy chain (motor domain) in yellow color, is followed by a stalk with black lines and light chains in purple. [7]

2.1.2.1 Kinesins

There were over 600 sequences of kinesins discovered in cells, including 45 kinesins identified in humans and mice; this large number led to a summary of nomenclature. On the first position is the name of the large family, in this case, kinesin, followed with a number from 1 to 14. [8] The first purified motor protein was kinesin-1, which occurs in squid neurons and carries organelles along the microtubules toward the plus end. The construction is made of N-terminal domain, which can be divided into the neck linker and neck region, the central stalk domain and C-terminal tail. [4]

In different kinesin families, the motor domain can be located at different places depending on the function. According to its location, the families can be classified as N-type (motor domain is located on N-terminal), I-type (internal location) and C-type (C-terminal location). [8]

2.1.2.2 Kinesin motility

Kinesin motors can be categorized based on several properties, their motility is categorized mainly according to a direction of the movement on polarized microtubule and processivity. Correlation between the direction of movement and the domain organization has been investigated for most of the motor proteins. All minus end kinesins have their motor domain C-terminal to the stalk as example kinesin-14. [9]

Processivity of the motors is determined as an ability to walk before their dissociation from the microtubule. It can be also described also as a number of ATP hydrolyses per microtubule-motor binding event. [9] Non-processive motors hydrolyze one ATP molecule and then dissociate from the microtubule. Conventional kinesin is a highly processive motor, it can walk more than one hundred of 8 nm long steps [9], on the other hand kinesin-14 is non-processive.

2.1.3 Kinesin - 14

Motor proteins from the kinesin–14 family are minus-end directed, non-processive motor proteins, essential as a part of bipolar spindle assembly, which is important for cell division. The members of the kinesin-14 family can slide antiparallel microtubules relative to each other. Kinesin–14, HSET, also known as KIFC1, has a common C-terminal tail domain, a central coiled-coil stalk and N-terminal globular motor-domain. [10] Their tail-domains associates with microtubules diffusively over longer time, in the order of minutes.

Kinesin-14 family members typically slide antiparallel microtubules relative to each other at a constant velocity. After reaching the ends of the fibres, they fully separate. In some cases, it is possible, that the connection remains stable for a short amount of time, but after several minutes it leads to the disintegration of the structure and separation.

2.1.4 Elasticity of DNA

Deoxyribonucleic acid shortly known as DNA is a bearer of genetic information. Double helix is typical for its structure which makes double-stranded DNA (dsDNA) stable. As all molecules, also DNA hods a conformation, which maximizes its entropy. By applying an external force on the molecule to stretch it, its entropy reduces. Such an elastic behavior is often described by the Kratky-Porod model also known as the worm-like chain model (WLC) [11]

2.1.4.1 Worm-like chain model

Worm-like chain is a model used to describe a behavior of semi-flexible polymers. In our case, we applied this model to a DNA molecule. The final mathematical expression for the force (F) related to fractional increase (x) is:

$$F(x) = \frac{k_B T}{L_p} \left(\frac{1}{4 \left(1 - \frac{x}{L}\right)^2} - \frac{1}{4} + \frac{x}{L} \right) \quad (1)$$

, where L is the length of the chain, k_B is the Boltzmann constant, T is the thermodynamic temperature and L_p is the persistence length of the polymer [12]. The WLC model provides a good description of the stretching of a DNA molecule, but the deviations appearing at higher forces renders the model unusable in this region.

2.2 Technical Background

In this chapter, I describe the essential methods and principles, which were used during my experimental measurements. For my study, basic training and understanding of the optical tweezers device and total reflection microscopy were most important. I had to understand, how those devices work and how to prepare samples for our experiments to obtain proper image results. Further I explain those techniques in sufficient detail considering the scope of this work.

2.2.1 Optical tweezers

Optical tweezers are highly-sophisticated machines invented for object manipulation in the microscopic scale. They were first realized by Arthur Ashkin and his colleagues at Bells Lab in 1986, under the original name single-beam gradient force trap. In 1970 they first observed, that the light causes a radiation pressure, that is able to push and accelerate small particles and under special circumstances able to trap them [13]. This phenomenon could be analysed in detail with the advent of new lasers. In early history, before the invention of lasers, we could find practical example of the radiation pressure in combination with movement only in the astronomical realm, where radiation pressure plays an important role for moving of matter. With the coherent source of light, the new opportunities appeared. They observed, that the coherent light can produce force large enough for moving the cells and particles of several micrometres in diameter. [14]

One of the most useful applications of the trap is force measurement, which is facilitated by the fact, that a spherical object is used for the manipulation. The force might be calculated from a displacement of the trapped object from its equilibrium position. The resolution of the force is in pN (10^{-12} N) range with detection of nm (10^{-9} m) displacement.

2.2.1.1 Construction

Lasers in near-infrared wavelength are used as a radiation source for traps, which have less photo-destructive effects on biological constructs and do not influence the imaging in the visible range. Basically, the machine is composed of a microscope with an objective of high numerical aperture, sensitive cameras for imaging, microscope with bright field, phase contrast or DIC illumination with condenser or detection lens. Besides those parts, for imaging of small single molecules, it is customarily supplemented with the fluorescent instalment of a commercially available microscope, featuring excitation lasers with a

different wavelength or a white light source lamp with dichroic mirrors and spectral filters. [14]

For trapping laser, in addition to wavelength and power, beam profile is crucial, and must produce Gaussian TEM00 mode [15]. Laser light is transported through a beam expander, a series of lens and mirrors, which is intended to spread the beam to larger diameter, so that the beam overfills the back-focal plane of the trapping lens. [14] The whole system is very sensitive to correct focusing and exact passing of the beam line.

2.2.1.2 Forces

Forces applied in optical tweezers arise from interaction between a collimated laser beam and a spherical particle. As was said, the laser is a coherent source of photons moving in the same direction of action. All photons in the beam have the energy of

$$E = h\nu \quad (2)$$

where h is the Planck's constant and ν is the frequency of the electromagnetic wave. For photons of specific wavelength λ , the momentum of a single photon is given by

$$p = \frac{E}{c} = \frac{h}{\lambda} \quad (3)$$

It is the change of light momentum through light-matter interaction that causes pressure, in this case radiation pressure. Mostly there are two main interactions exerting forces upon the object – reflection and refraction. Based on that we often divide total applied force into two components – the scattering force, in the direction of light propagation and the gradient force in the direction of the spatial light gradient. Such decomposition is convenient, since both face a different direction. In order to achieve effective trapping, gradient forces must exceed simultaneously applied scattering forces. [16] [17]

To move from a single photon to entire beam we need to consider whole angular momentum flux of the beam. Momentum flux of the beam in direction of the ray depends on its power P , or energy flux, and refractive index of the medium n , where the ray is moving and c is the speed of light.

$$p = \frac{nP}{c} \quad (4)$$

The momentum flux is dependent on the beam geometry. For axial forces the more the beam is divergent or convergent, the lower is the momentum flux. [17]

Based on the relative size of the object and used wavelength we can distinguish three major approximations – Rayleigh, Mie and generalized Lorenz-Mie theory. Rayleigh approximation is applied to particles much smaller than the wavelength of the used light, Mie calculations work for spheres much larger than the wavelength and the Lorenz-Mie theory applies for objects having a similar size as the wavelength of the laser. [18] [19]

2.2.1.3 Mie optic ray regime

The physical foundations are most obvious for particles in Mie size regime (diameter of a particle is larger than the wavelength). It is feasible to use simple ray optics to describe the scattering and optical momentum, where the light beams are possible to decompose into individual rays with intensity, direction, and state of polarization. Each ray follows Snell’s law of refraction and Fresnel’s equation for transmission and reflection.

For calculation, spherical particles are used with higher refraction index than that of the surrounded medium, otherwise the gradient force cannot influence the particle in right direction for trapping. The advantage of a spherical surface is, that the description in ray optic is uncomplicated and the forces can be uniformly distributed.

Ground for it is based on Snell’s law of refraction, which describes, how the beam behaves at the interface of two media with different refraction index. When the beam of light is incident on the interface of two transparent media with different refraction index, in general, some of the light is refracted into the second media and some of it is reflected, and its momentum will change.

$$\sin(\theta_1) \cdot n_p = \sin(\theta_2) \cdot n_m \quad (5)$$

, where n_m is refraction index for surrounded medium (typical is used ~ 1.33) and n_p is refraction index for the material of trapped particle (~ 1.5). The angle of incidence is θ_1 and the angle of refraction θ_2 . Laser wavelength is within the infrared part of the spectrum, mostly 1064 nm, because of the low biological absorption.

We stated earlier that scattering and gradient forces come from reflection and refraction respectively. Reflection pushes the object in the direction of light propagation, and as such it is not very useful as a trapping force, when considering optical trap consisting from just a single laser beam. Gradient force caused by refraction heads toward the change of the momentum induced by refraction on the interface of the object and its surrounding medium. Such situation is visualized in Figure 3, where two rays (a and b) from laser

beam are reflected on the dielectric spherical particle. Forces F_a and F_b are the gradient forces and by the Newton's third law they are oriented against the change of the ray direction. The sum of those vectors is the force F , which will always point towards the laser focus f . This is the main principle used in single laser beam traps and the reason why gradient forces must dominate over the scattering forces in order to achieve effective trapping. Since we can't eradicate the scattering forces entirely, the actual centre of the trap would be slightly shifted from the ideal position, which is identical with laser focus. [20]

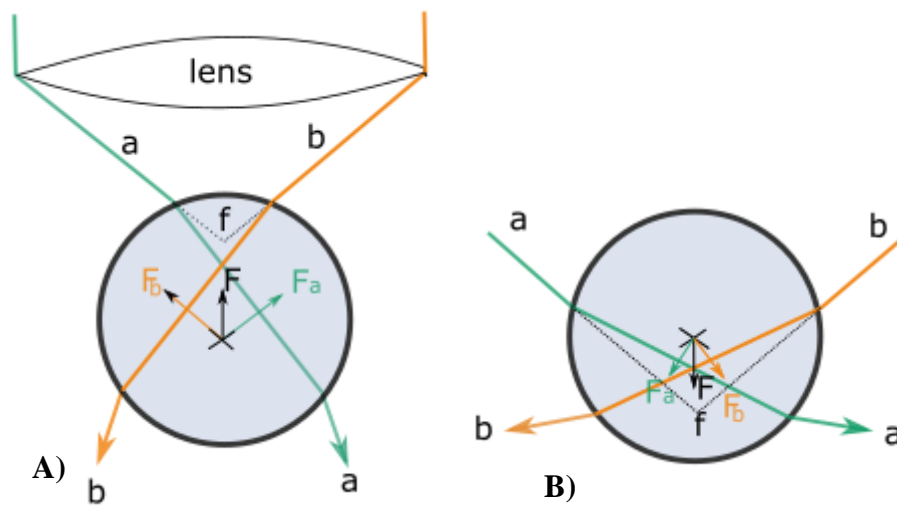


Figure 3: Trapped beads in focused laser beam

Illustration of a microsphere particle trapped in focused Gaussian laser beam (modeA TEM00) with high NA objective. Arrows represent the directions of gradients forces components (F_a and F_b .) (Figures are taken over by [15]).

The gradient force doesn't just keep the object in the focus, but also functions as sort of autocorrective mechanism, that retrieves the object back into the focus when displaced. This property depends on the beam geometry – the larger numerical aperture (NA) of the focusing lenses we use for collimation, the more we improve the trapping ability. Such displacement autocorrection is described in Figure 4.

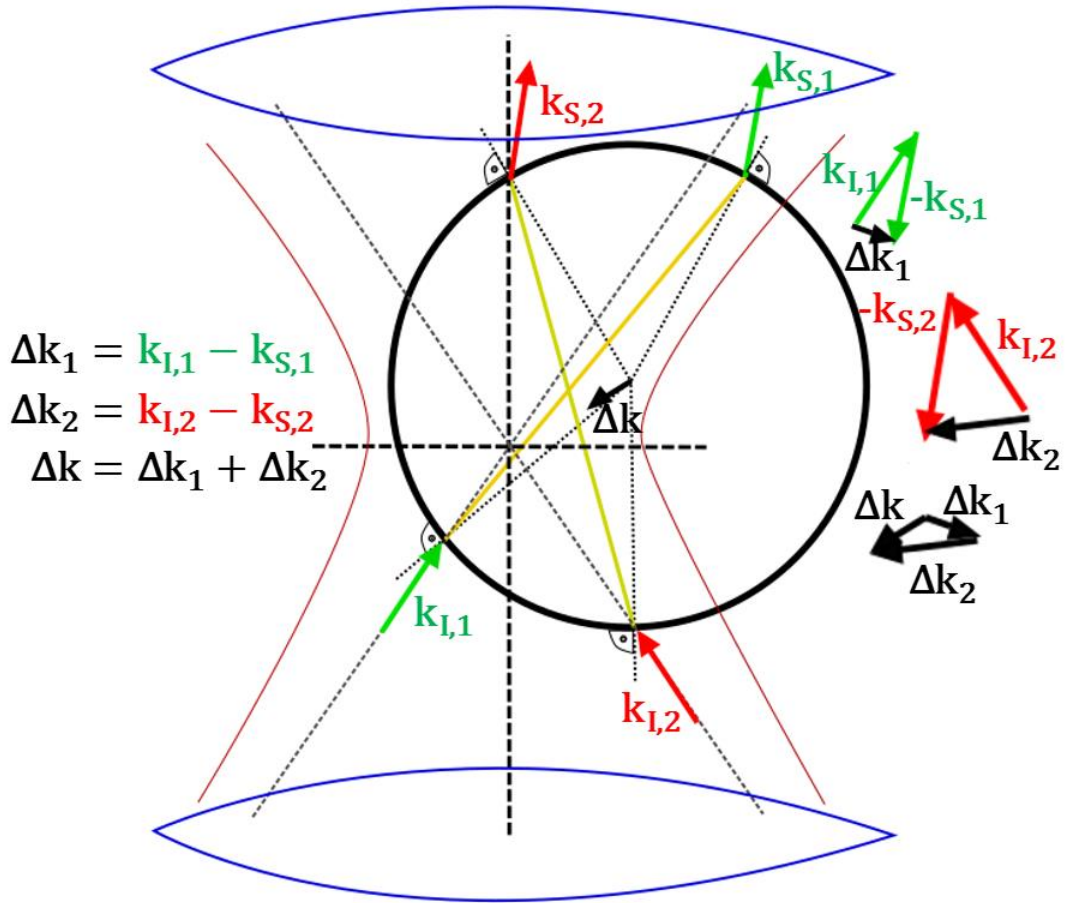


Figure 4: Dielectric sphere displacement

When the dielectric sphere has been displaced from the laser focus, the sum of the gradient forces applied will point in the direction of the focus, correcting the displacement. In this case, the forces arise from refraction of two incoming rays $\mathbf{k}_{I,1}$ and $\mathbf{k}_{I,2}$ causing a momentum change $\Delta \mathbf{k}_1$ and $\Delta \mathbf{k}_2$ of two outgoing rays $\mathbf{k}_{S,1}$ and $\mathbf{k}_{S,2}$. Total pull towards the centre of focus is then represented by $\Delta \mathbf{k}$. (Figures are taken over from [21])

As was described above, we can influence the overall trapping ability of the optical trap by altering some of its parameters. Aside from NA, where the principle is the bigger the better, we can also improve the tracking by increasing the laser power. Other than that, the size of the object, polarization of the light and refractive indexes of the object and its surrounding medium can also impact the trapping. [22]

2.2.1.4 Force detection

Forces corresponding with trapped objects are extremely small (order of pN), applied on a range of different object sizes from nm to μm and could manifest over a short time period. Measuring such forces could pose a serious challenge, but things are less complicated because of the direct dependence of the trapping force and relative position

of the object to the laser focus. This dependence can be expressed in an adaptation of Hook's law

$$\vec{F} = -k\vec{x} \quad (6)$$

where \vec{x} is the relative displacement and k is constant called "trap stiffness". Practically all we need for being able to successfully measure optical trapping forces, is a position detecting system and characterization of our trap's stiffness.

There are several methods to measure relative displacement of the object. Easiest could be to setup video imaging system to microscope, and observe the object directly. While this could yield sufficient resolution for most applications (typically $\sim 10nm$), the method suffers from inadequate video acquisition rates (from 25Hz to $\sim 125Hz$) and is subjected to other conditions that affect the final resolutions such as illumination or time jitter. This could be partially solved by the use of high speed rate cameras, but moving into the kHz or even MHz area puts high pressure on the computing system, data storage and various algorithms to extract the distance information from the image. [23]

Other methods involves the use of additional laser system, combined with quadrant photodiode detector (QPD) for direct position observations, but ideally, we would like to use the trapping laser itself to perform the measurement. This can be done through technique called back-focal plane (BFP) interferometry. It uses interference of the trapping non-scattered light with the light that has been scattered by the displaced object from the focus. This causes a shift in the laser spatial intensity and most importantly a small phase shift. Given the amplification of the signal interference, this approach produces an impressive sensitivity – even if only 1% of the incident light is scattered, produced interference signal is still 20%. To quantify the interference pattern, the back-focal plane is imaged on QPD – visualization of such situation can be seen in Figure 5. Unlike video imaging, the BFP interferometry tracking on QPD allows detection at MHz rates up to 100MHz and Angstrom resolution. [24]

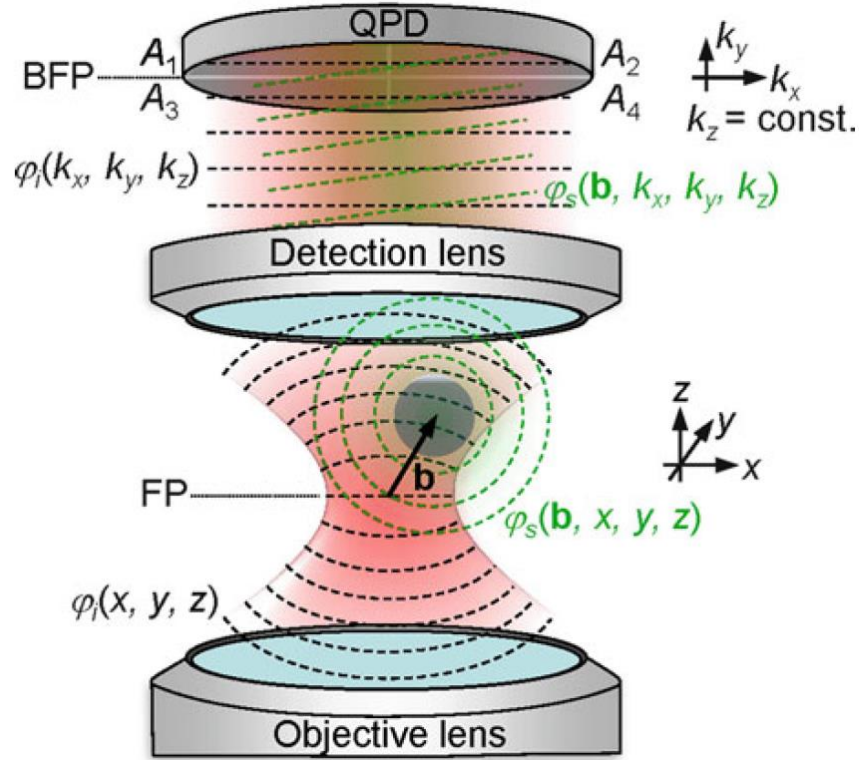


Figure 5: Back-focal plane interference pattern

Illumination of BF plane interference pattern on QPD detector. Bead is in a position \mathbf{b} relative to the focus. (Figures are taken over from [25])

2.2.1.5 Calibrations

In previous chapter, we described the proportionality between distance displacement of the object and the trapping force through a constant trap stiffness. There are several approaches to obtain this trap stiffness, usually involving viscous drag calculations. In our system by Lumicks we used Power-Spectrum approach for the calibration, which analyses the fluctuations of a bead particle trapped inside the laser beam. The displacement of particles is detected by using back-focal-plane interferometry. The signal of the laser beam, which is scattered by the microsphere, is detected and measured by a quadrant diode or PSD (position sensitive detector). Measured spectrum is fitted by Berg-Sørensen & Flyvbjerg method [26].

Generally, this method could be called Brownian motion calibration, since the motion detected on the PSD is a consequence of thermal fluctuations. First we need to measure the power spectrum, which is in essence frequency dependence of thermal fluctuations. Such spectrum is represented in Figure 6, where the y-axis is described through the detector response and horizontal axis provides the frequency. We can clearly see that at

low frequencies the fluctuations have almost constant mean amplitude until the *corner frequency* is reached, after which the slope of the spectrum decreases drastically as the high-frequency fluctuations are increasingly damped (Figure 6). The corner frequency is the initial parameter needed to express the trap stiffness k (pN/m)

$$k = 6\pi^2\eta a f_c \quad (8)$$

where a stands for the sphere's diameter, f_c is the mentioned corner frequency and η is the dynamic viscosity of the object surrounding fluid. Further parameters must be known for precise measurement, namely detector's distance response C_d ($\mu\text{m}/\text{V}$) and from that derived force response C_F (pN/V). We can calculate the distance response as

$$C_d = \left(\frac{k_B T}{3\pi^2 \eta a (S_0 f_0^2)} \right)^{1/2} \quad (9)$$

where k_B is the Boltzmann constant, T represents thermodynamic temperature of the medium, $S_0 f_0^2$ ($\text{V}^2 \text{Hz}^{-2}$) is the low frequency plateau of the power spectrum. From here we easily write for the response

$$C_F = k C_d \quad (10)$$

All those necessary parameters are subsequently derived from the power spectrum, as we can see in individual results from the right side table in Figure 6. [26]

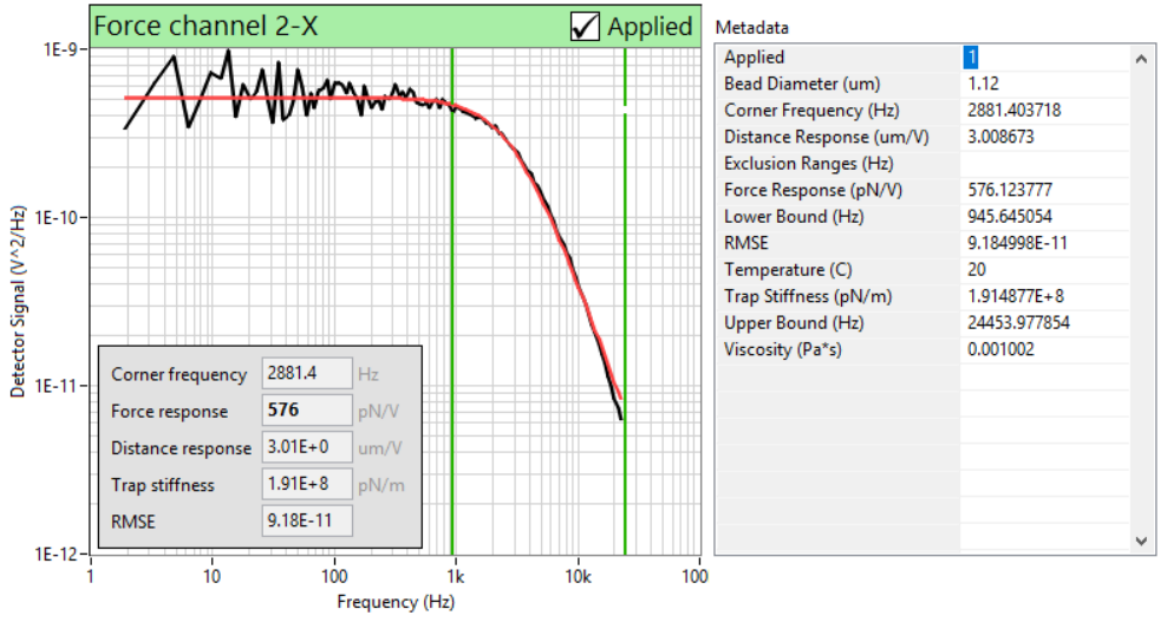


Figure 6: Power spectrum

Example of power spectrum obtained for our optical tweezers device for one trap during the calibration phase. (Lumicks)

2.2.2 Microscopy techniques

In this chapter I focused on short description of the mechanisms of microscopy techniques used in my work. Total internal reflection microscopy (TIRF) was used for the investigation of the kinesins behaviours and next to it, the optical tweezers device is combined with the confocal scanning microscopy and a bright field microscope is present for the beads illumination.

2.2.2.1 Light microscopy

The background of modern light microscopy was founded around 70's of the 19th century by Erns Abbe, who demonstrated diffraction of light by the objective lens and determined the resolution of the image for samples. He defined the mathematical relation for numerical apertures (NA) of condenser and objective with the wavelength of the light used for imaging. It defines the resolution of an optical microscope as the minimal distance between two points of the image, at which they can be still distinguished.

$$d_{min} = \frac{1.22\lambda_0}{NA_{obj} + NA_{cond}} \quad (15)$$

, where d_{min} is the minimum lateral distance that can be resolved, λ_0 is the wavelength of the used light for imaging in a vacuum. NA are numerical apertures of objective and

condenser, it defines the range of angles, at which the objective or condenser is able to accept or emit light.

For the description of the best-focused points Airy disks are used in the diffractions pattern, where the radius of the brightest centre (r_{Airy}) is given by:

$$r_{Airy} = 0.61 \frac{\lambda_0}{NA_{obj}} = 0.61 \frac{\lambda_0}{n \sin \alpha}. \quad (16)$$

, where NA_{obj} is numerical aperture of the objective, equal to $n \sin \alpha$, where n is refraction index of the medium surrounded the lens and α is the half of the maximal angle of the cone of light that can enter or exit the lens.

One of the simplest light microscopy techniques might be bright field microscopy, which is used in my work for visualization of trapped beads. The principle of forming the images from bright field microscope comes from absorbance of light by the sample. The source of the light is placed from one side and the detector from the other. Next to the conventional light microscope, popularity of the fluorescent microscopy is booming. [27]

2.2.2.2 Confocal laser scanning microscope

Confocal microscopy is a technique, which is able to increase the optical resolution with help of spatial pinhole filter. Spatial pinhole filter is used for the removal of unfocused light, which causes parasitic effects on images. This technique is widely used for biological imaging of fluorescently labelled samples, instead of a conventional fluorescent microscopy.

For conventional fluorescent microscope, the whole sample has to be exposed to radiation at the same time and there are no possibilities to choose a small part of our object for imaging. This may cause faster photo-bleaching and degradation, but also all layers in Z-plane are detected at the same time and are illuminated in the obtained image. Compared to that, confocal imaging uses laser light, which can be focused only in the plane of our interests and subsequently detected fluorescent signal only for the proper Z-plane and obtain the image clearly, without any unwanted information from the other planes.

Confocal microscopy falls among scanning techniques, the imaging laser scans point of the sample after point and detects the information of fluorescence photons. The final image is constructed of the points with information about the fluorescence intensity with time drift. An important characteristic, which can be a small disadvantage, is the speed of

scanning and imaging. It varies per device. It depends on optical properties such as numerical aperture, size of the scanning area (obviously for imaging of larger area, more time is needed), quality of image (pixel size, resolution and levels of grey, the amount of light applied to point etc.). [28]

2.2.2.3 Total Internal Reflection Fluorescence Microscopy

Total internal reflection fluorescence microscopy, shortly TIRF, is a method which allowed us to image a single motor protein moving along a microtubule. Laser light is used as a radiation source in TIRF microscope, which shines on the coverslip surface at critical angle. At critical angle, total internal reflection can be observed. The light is reflected from the coverslip and does not pass through the whole sample; only the small area near the surface is illuminated by the evanescent field. Thanks to the existence of this phenomenon, the excitation of fluorophore is observed only near the area to the surface without background. [29]

2.2.2.4 Fluorescent labeling

Fluorescent labeling is important for visualization of samples smaller than visible wavelength used in conventional optical microscope. It is a molecule chemically attached to the sample under investigation. Fluorophore selectively binds to the function groups on the molecule and for this reason it is possible to also use it inside whole cells.

In my investigations, several types of the fluorescent probes were used. Figure 7 provides visualization of emission and excitation spectra of used fluorophores. For excitation, a laser or epifluorescence lamp is usually used, for the best fluorescent answer, the wavelength of the light source has to be close to the maximum, according to the spectrum. After the irradiation of the sample, the electrons are excited to a higher electron level and when returning to the lower electron level, a photon is radiated. In most of the cases, the photons emitted have a longer wavelength than the source of the radiation used for excitation. [27]

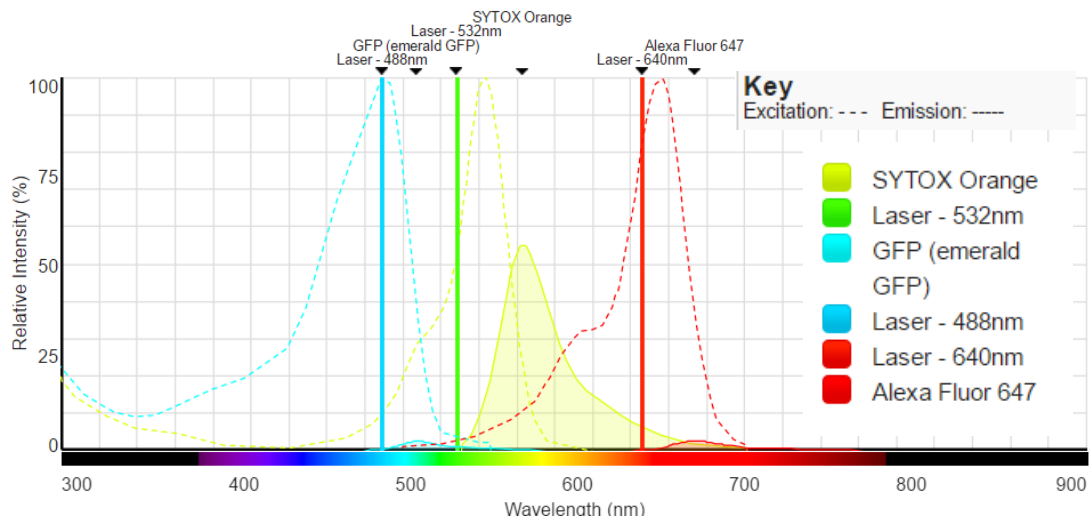


Figure 7: Emission and excitation spectrums.

In the image are three fluorescent emission and excitation spectrums (GFP, SYTOX Orange and Alexa Fluor 647 nm) used in our experiments. The excitation spectrums with dashed lines show the wavelength used for the excitation of fluorophores to a higher energy level. During the return to basic level, the photon with higher wavelength is emitted. This difference is known as Stokes shift. [30]

3 Methods and materials

First chapter is dedicated to the optical tweezers C-Trap and its parameters used for the measurement of DNA and entropic forces produced by kinesin-14 HSET. The following chapters describes the preparation of materials and experimental set up for two types of experiments with DNA and kinesin-14, HSET.

3.1 C-Trap optical tweezers

C-Trap device is optical tweezers device from Dutch company Lumicks. Using Nd:YAG laser with TEM₀₀ mode and 1064 nm wavelength in infrared spectrum for trapping. Infrared spectrum lies in a region, where cells have a low absorption level. The trapping laser is led through a path with a series of optical components that correct the beam into proper size and shape and through splitters it is possible to obtain up to 4 traps. Each trap is moveable by rotating a steerable mirror. The trapping laser path is directed through exit water immersion objective, where the sample is placed.

In Figure 8 a visualized schematic image of components inside the C-Trap device is shown. The trapping laser is split into up 4 orthogonally polarized optical traps with independent moving mirrors. Positions of beads are recorded by bright field microscopy provided by CMOS camera (875 nm). For the fluorescent imaging is implemented series of three confocal imaging lasers with 640 nm (red), 543 nm (green) and 467 nm (blue) wavelengths. The deflection of the beads inside traps, necessary for the force measurement, is provided by two position-sensitive detectors (PSDs). Their functions are described more deeply in chapter focused on optical tweezers.

In Figure 9 are pictures of the C-Trap components necessary for illumination of the samples. The water immersion objective (Figure 9-1) is placed from the bottom of the sample and according to the reflection (Figure 9-2) the laser beams is focused inside the flow cell. The oil immersion condenser (Figure 9-3) is placed from upper side of the sample. In Figure 10 is an example of the inbuilt LabView software for manipulation and force measurement.

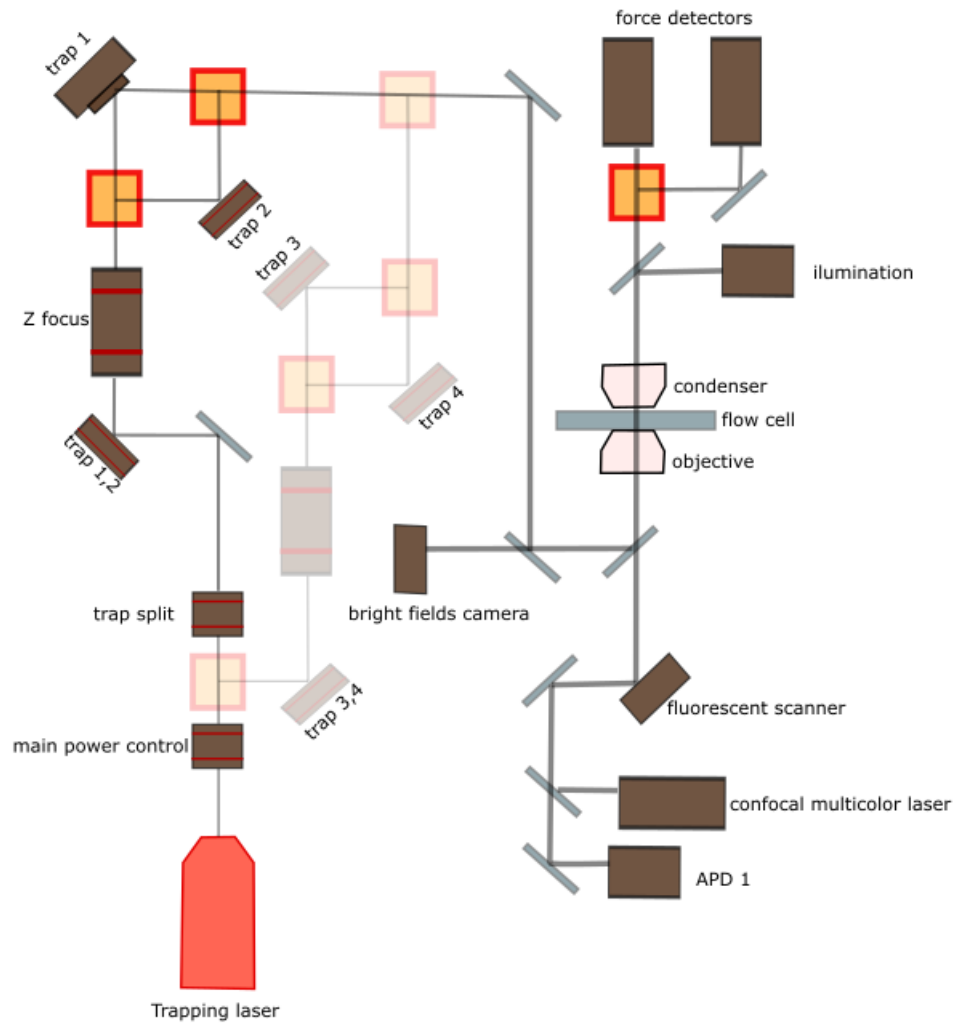


Figure 8: Schematic diagram of the C-Trap device.

Schematic image of the C-Trap device shows us the main components used for the construct of the optical traps. As a source is used Nd:YAG (1064 nm), which is lead through a series of optical units. Two or four orthogonally polarized optical traps are independently steered using mirrors. The deflections of the beads inside traps is measured by force detectors, in our case are used two position-sensitive detectors (PSDs). The beads are illuminated by bright field camera. For fluorescent imaging are presented excitation beams with wavelengths 640 nm, 543 nm and 467 nm.

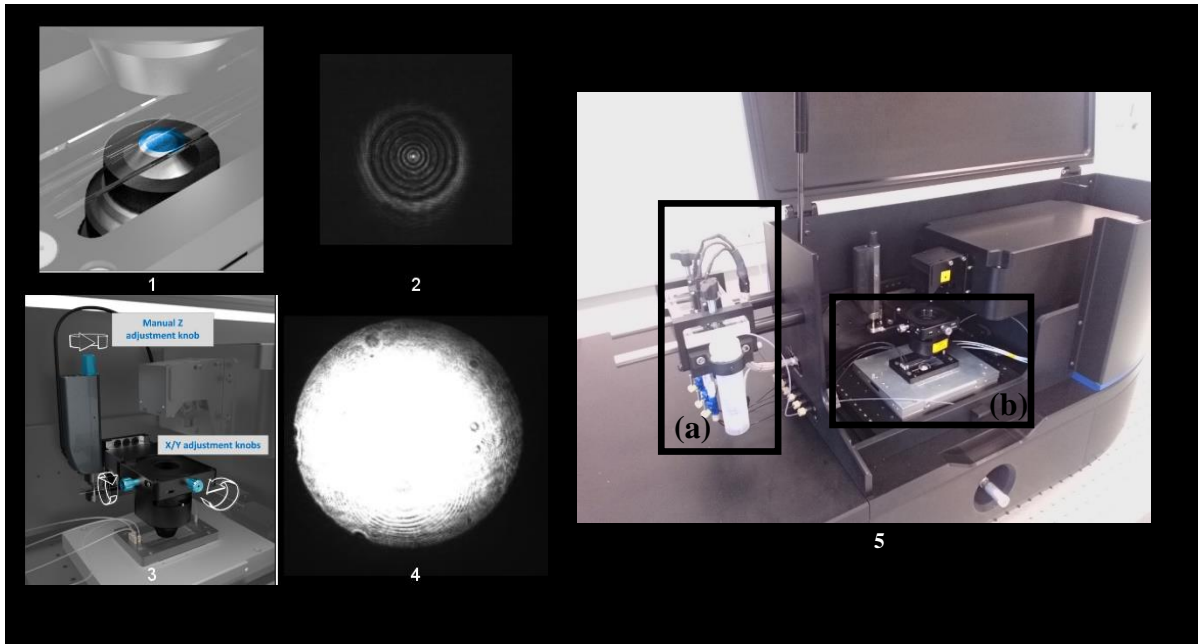


Figure 9: Optical tweezer C-Trap

(1) Water immersion objective forms the optical trap and fluorescent imaging placed below the sample stage. (2) image of the reflection caused by laser light from the objective on the surface of the glass flow cell. (3) Oil immersion condenser placed from the top of the sample stage. (4) Illumination from the condenser for aligning of the proper position. (5a) Microfluidic system by LUMICKS with pressure chamber for performing a laminar flow inside the flow cell. (5b) Piezo sample stage used for manipulation with sample and calibration of the movement.

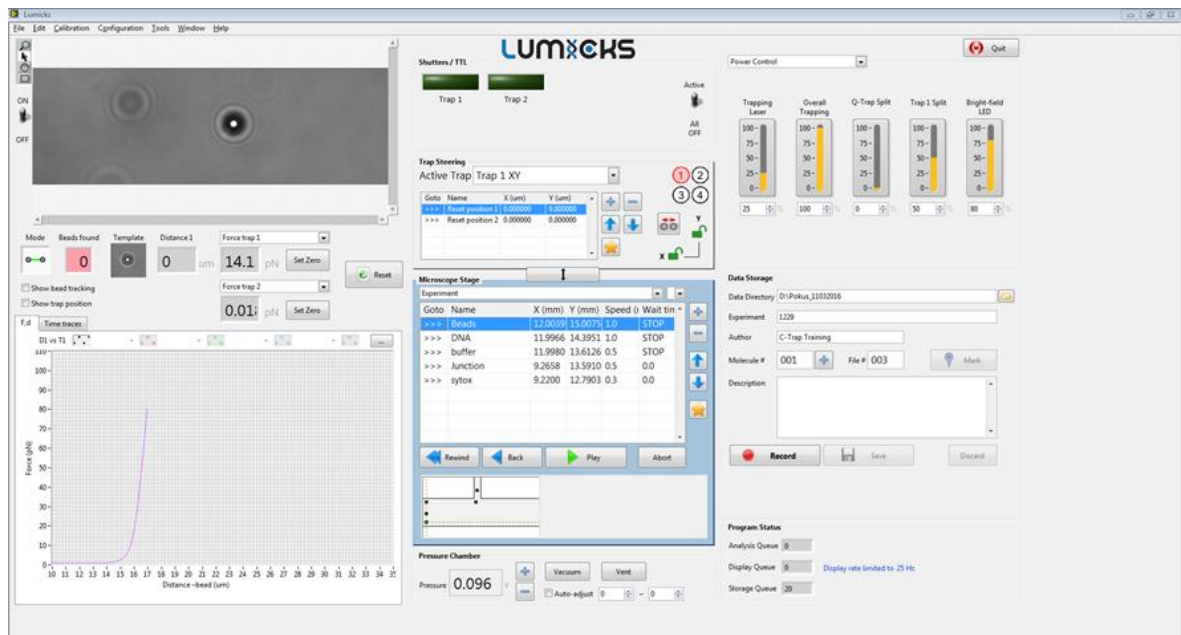


Figure 10: Inbuilt LabView software for optical tweezer

The print screen of the software used for the optical tweezer experiments with bright field illumination for manipulation with beads and force spectroscopy measurements. (Lumicks)

3.1.1 Microfluidic system

Samples are placed in syringes connected with microfluidic system. Microfluidic system is important for ensuring stable conditions. Most of the experiments, which are provided, have biological character and it is necessary to work with living materials. Buffer solutions and samples are therefore refreshed by the flow inside multiple channel chip. This system works as a closed unit without access to the external environment and under constant pressure, the conditions are restored over time.

Microfluidic system is permanently connected to the optical tweezer device and ready for measurement. The outside part consisted of pressure system and syringes with samples. The inner part is interconnected through tubing system with syringes, where we can easily restore solutions. The microfluidic system contains elaborated glass chip with channels, for easy non-contact manipulation with assay parts. In Figure 11a we can see a schematic drawing of the glass chip from the upper view. In Figure 11b the multichannel flow cell is visualized from the side view, to see the position of the reflection used for manual focusing the objective.

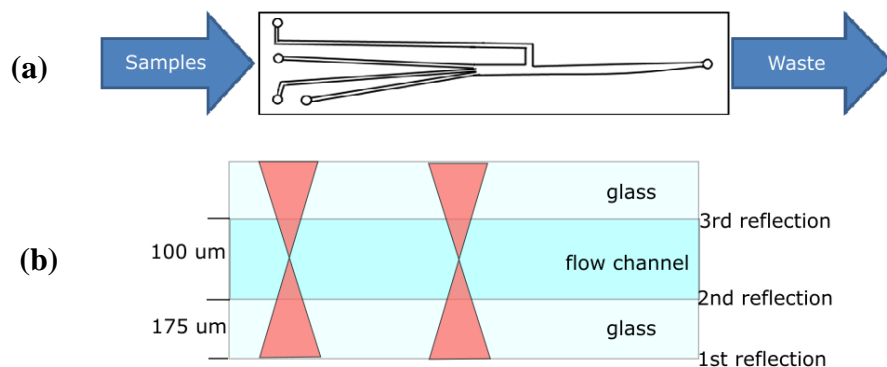


Figure 11: 4 channel laminar flow cell

(a) Flow cell with 4 channels for samples used for optical tweezers experiments with DNA and microtubules. (4 entrances for samples and 1 exit for waste) (b) Schematic side view of the flow cell with 2 traps (visualized by red color) and dimensions for the proper setting of trapping laser position and piezostage. Reflections are used for manual focusing of the objective into the sample flow cell. (Lumicks)

3.2 DNA experimental set up

Lambda phage DNA elasticity was performed on optical tweezers with 4 channel laminar flow cell with two traps. In optical tweezers experiments, a single strand of the DNA molecule is bound by chemical attachment to the surface of coated beads, which serve as a tool for manipulation with the molecule, without destroying its structure by laser power. It is possible to tether the molecule of DNA between two beads or with one of the end the surface of coverslip. In my experiment two beads set up was used, where the interaction area is only on the surface of beads.

As beads were used polystyrene beads 3.5 μm in diameter (Figure 12). Traps can easily move between channels of the laminar flow cell (Figure 11). The microfluidic system provides us with easy and fast change of the buffer and samples and ensures the laminar flow between channels with segments of the assay and thanks to no mechanical barriers, we can easily reach the required position.

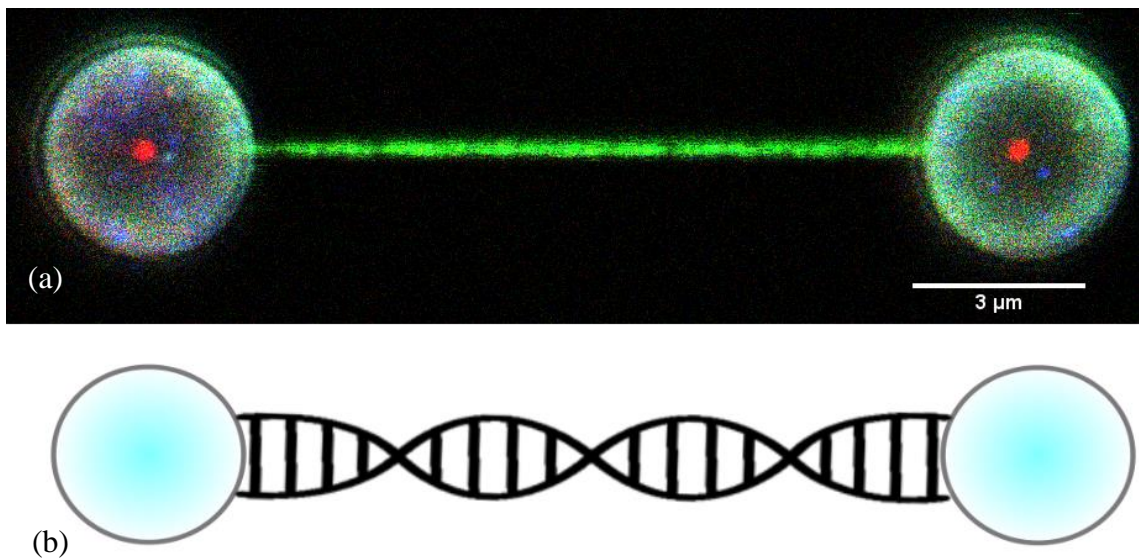


Figure 12: Tethered molecule of dsDNA.

(a) Confocal microscopy image of lambda DNA labeled by SYTOX Orange (excited by 543 nm) at 100 nM and tethered between 3.5 μm in diameter polystyrene beads and (b) illumination of the situation.

As sample chamber, we used four channels chip with laminar flow described in previous chapter. Layout of channels inside the flow cell (Figure 13):

1. beads in concentration 1:1000 (beads: PBS buffer)
2. DNA in PBS
3. PBS
4. Sytox Orange

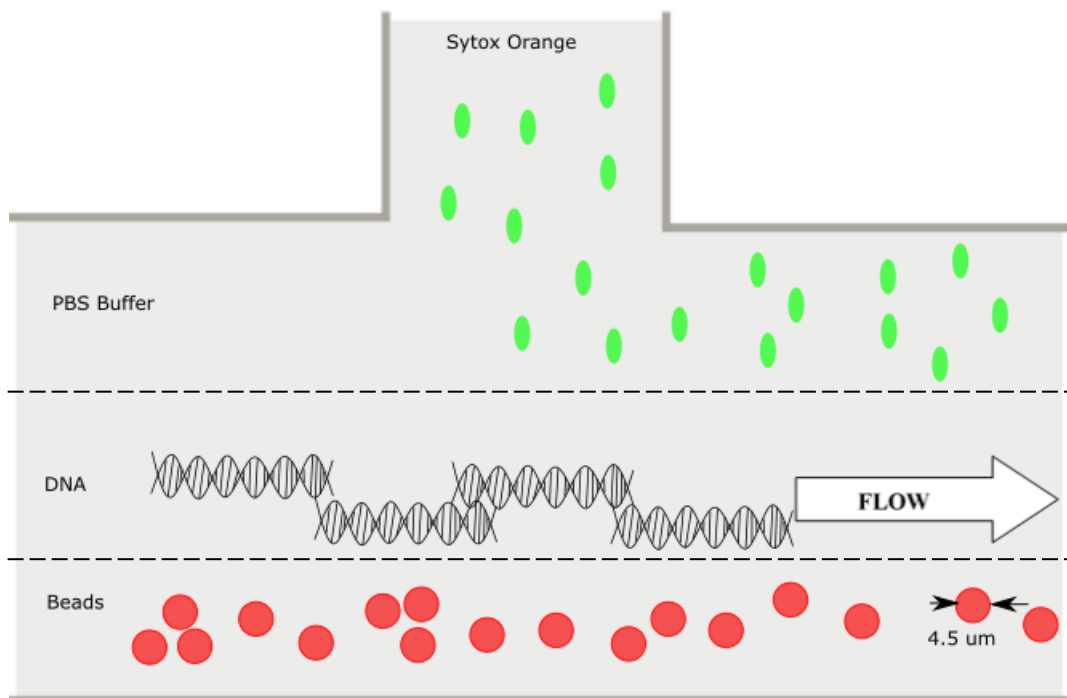


Figure 13: Layout of positions inside flow cell for DNA.

The upper view of the multichannel flow cell for the DNA and Sytox Orange in PBS. The first channel contains polystyrene beads (3.5 μm in diameter Spherotech), the second channel DNA in PBS, the third channel PBS and the fourth one Sytox Orange in PBS.

3.2.1 DNA fluorescent probe

The excitation of fluorescent probe dye can lead to the production of reactive oxygen and free radicals, that can lead to breakage of the DNA and as such needed to deal with. To solve this issue, the concentration of the fluorescent dye can be reduced or alternatively it is possible to use oxygen scavenger (enzymes species interacting reactively with oxygen), which should positively affect the intramolecular interaction in DNA molecule and make it more stable. [31]

For this reason, in further experiments we used the oxygen scavenger (OxSc), usually used to delay the photobleaching effect and reduce the photo-damage of biological

samples. As an oxygen scavenger, we used glucose oxidase (in concentration 0.22 mg/ml) and catalase (in concentration 0.02 mg/ml) and glucose (in concentration 20 mM).

3.3 Kinesin – 14 HSET experimental set up

For experimental investigation of crosslinking activity, green fluorescence protein (GFP) HSET was purified by affinity chromatography. For the experiments, we prepared tubulin purification from porcine brain. Some of the tubulin was labeled with Alexa 647 or biotinylated. For experiments were used 3 different mix type of porcine tubulin in concentration ratio 1:1:30 (biotinylated: Alexa 647 labelled: biotinylated tubulin) in final concentration 5 mg/ml for illumination and catching with optical tweezers. Second tubulin mix in ratio 1:50 (labelled: unlabeled tubulin) and third tubulin mix in ratio 1:50 (biotinylated: unlabeled) in final concentration 4 mg/ml. Microtubules were double stabilized with taxol and GMPCPP (Attachment 2). For experiments with optical tweezers we used polystyrene beads 4.5 μm and silica beads 1.12 μm (both Spherotech).

3.3.1 TIRF experimental set up

For the TIRF microscopy part of the study microfluidic chamber was prepared, from two 18mm and 22mm cover slips (Corning 2845-15 and 2845-22), which were held together with strips of melted parafilm. In Figure 14 I have visualized the holder and the cover slip used for the experiment. Those coverslips are specially modified with DDS coating procedure for sticking the samples to the surface. The TIRF microscopy imaging used only a small area near the surface and immobilization of the molecules is elementary. DDS modified microfluidic chamber is coated with antibodies and immobilized microtubules to the surface.

For studying the GFP-HSET behavior during crosslinking we employed biotin antibody for the coating of the cover slip surface. Incubated with pluronic F-127 (100 mg/ml in BRB80), a difunctional block copolymer surfactant. After finishing the surface treatment, biotinylated template microtubules in BRB80 with taxol (80 mM Pipes/KOH pH 6.9, 1 mM MgCl_2 , 1 mM EGTA, 10 μM paclitaxel) and are bound to the surface of coated cover slip. Those immobilized microtubules serve as a path for the GFP-HSET.

At first, we prepared a motility buffer (MB) with ATP to investigate the ATP-dependent movement properties of HSET and then with ADP for inactivation of the motor part of the kinesins and investigating the ATP-independent motion (20 mM HEPES pH7.2, 1mM

EGTA, 75mM KCl, 2 mM MgCl₂, 1 mM ATP/ADP (+Mg), 10 mM dithiothreitol, 0.5mg/ml casein, 10 μM paclitaxel, 0.1% Tween, 10% w/v sucrose, 20mM d-glucose, 110 μg/ml glucose oxidase and 20 μg/ml catalase). After flushing microtubules with motility buffer and GFP-HSET, the fluorescent labeled microtubules were added and the interaction was observed.

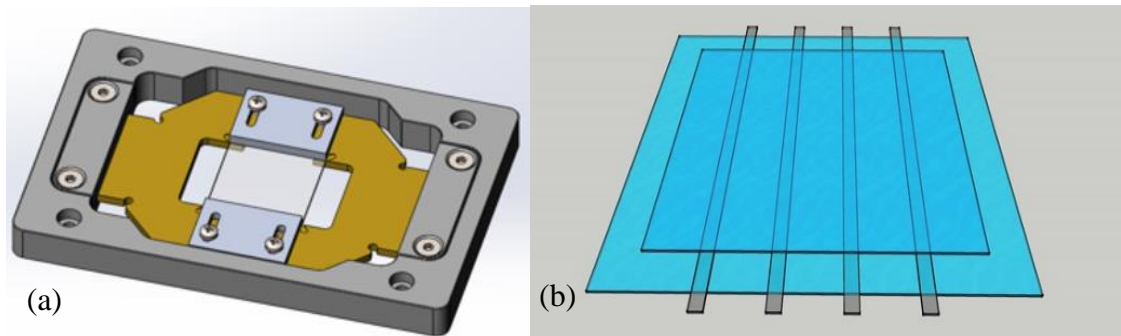


Figure 14: Sample holder and microfluidic chamber.

(a) The sample holder used for coated microfluidic chamber for using inside the optical tweezers with confocal imaging. (b) The schematic image of used microfluidic chamber for the microtubules experiments composed of 18x18 mm and 22x22 mm cover slips.

3.3.2 Optical tweezers experimental set up

To measure forces, I used optical tweezers combined with confocal microscopy. I created partial microtubule overlaps by attaching two microtubules to two silica beads and bringing the two beads in close proximity using two optical traps in presence of GFP-HSET and ADP in solution.

After the overlap was established, I pulled the two microtubules apart by stepping movement of one of the traps relative to the other. Immediately during the measurement, the force curve could be observed.

The chemical conditions were prepared and tested during the TIRF microscopy, for the microtubules and GFP-HSET solution was used MB with ADP and OxSc, the motor domain was inactivated. Sensitivity and stiffness of the trap were determined using an inbuilt calibration feature that fits a Lorentzian function to the power spectrum of the thermal fluctuations of a trapped bead.

Measurements were performed at a trap stiffness of 0.231 pN/nm with the optical power of a 1064 nm trapping laser. The time traces were recorded with 1 kHz sampling rate. The

time traces were further analysed and converted into force-distance curves using an in-built software. During the force measurement, microtubules and GFP-HSET were visualized by confocal imaging using 488 nm and 647 nm excitation wavelengths (LUMICKS).

As sample chamber was used the four channels chip with laminar flow described in previous chapter 3. Layout of positions inside the flow cell for GFP-HSET experiment (Figure 15):

1. beads in concentration 1:1000 (beads: BRB80 buffer)
2. microtubules with motility buffer and oxygen scavenger
3. motility buffer with oxygen scavenger
4. GFP-HSET in concentration ratio (1:3000)

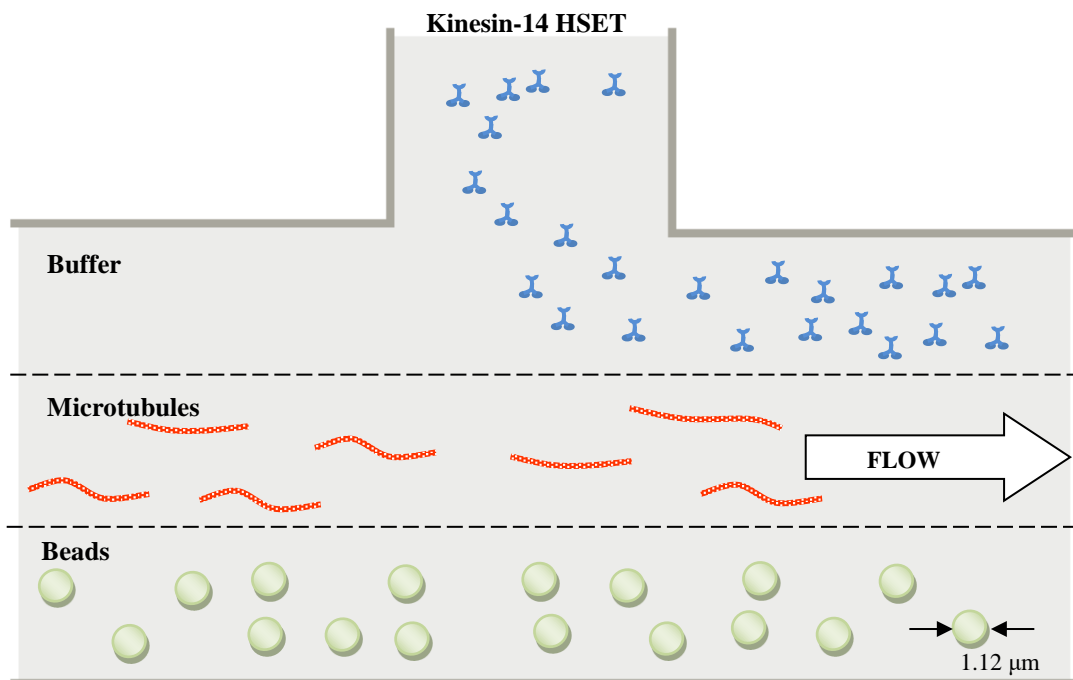


Figure 15: Schema of flow cell with the assay for GFP-HSET experiment.

The upper view of the multichannel flow cell for the microtubules and GFP-HSET experiment with optical tweezer. The first channel contains silica beads (1.12 μm in diameter Spherotech), the second channel GMPCPP-stabilized biotinylated Alexa 647 fluorescent labeled microtubules inside MB, the third channel MB and the fourth one GFP-HSET in MB.

3.3.3 Correlation of fluorescent imaging with force measurements

For raw results analysis, it was necessary to correlate image sequence with force curve. The software delivered with the tweezer can record image sequence and force curve information in two different files, but without the correlation of time from both files, we cannot obtain a useful information about the behaviour of our system. Both records are made manually and it caused a small shift between both files. Based on this shift, we obtain the difference in time between both files and we can use it as a start time for calculation.

Next step is to obtain the time information from an image sequence, from where we derived how long it took to obtain a single line of the fluorescent signal from confocal microscope. This time line we can use to find a proper place in image, where the force was recorded. In attachment 4 and 5 are full matlab codes used for marking the image position onto the curve and vice versa. (Figure 16)

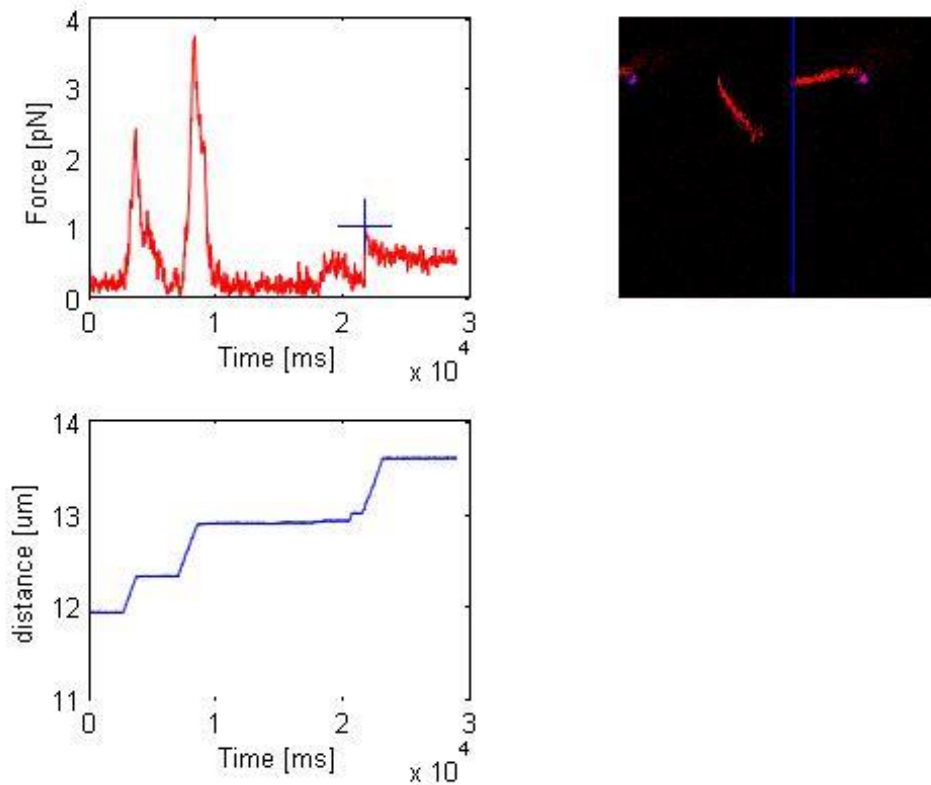


Figure 16: Example of result for correlation of time

The results from matlab code might be useful for correlation of the unusual situation of the force curve with the sequence of fluorescent images. In this case, an anomaly near the end of the recorded force curve was caused by separation of microtubules. The red curve shows us the force changes over time and the blue curve the distance changes over time. The image corresponding to the event labeled with blue cross in the red curve.

4 Results

The results part is divided into two larger chapters, where the first one is dedicated to experiments intended for initial proof-of-principle experiments using the optical tweezers with DNA and the second one aims at the experiments with cytoskeletal filaments and kinesin-14, HSET.

The chapter about DNA investigation included measurement of its elasticity and binding of DNA intercalator SYTOX Orange. It served as an initial test of the system software for force measuring and calibration. According to the obtained results, it was possible to start using the device for cytoskeletal structural proteins.

The kinesin-14, HSET experiments chapter shows the results taken with the help of TIRF and confocal microscopy. Initial experiments using TIRF microscopy were designed to illuminate the kinesin's behaviour in presence of ATP and ADP. Based on the observed kinesin behaviour, we have designed the following experiments using the optical tweezer device.

4.1 DNA investigation results

As was described in the Methods chapter, for the DNA experiment were used polystyrene beads of 3.5 μm diameter coated with streptavidin for tethering of DNA molecule. Two coated beads are trapped by orthogonally polarized laser beams and one molecule of dsDNA is tethered by biotinylated ends to them.

First I measured elasticity of the single DNA molecule and compared it with theoretical and expected results, provided by other groups around the world. The experiment with DNA-extension measurement was followed up by visualization of single fluorescent probe molecule, in my case SYTOX Orange, excited by 543 nm wavelength.

4.1.1 DNA Elasticity

Measurement of the elasticity of single molecule λ -dsDNA is performed by moving one of the beads, to which the molecule is tethered, in direction of increasing the distance between the traps for stretching and in opposite direction for relaxing. The force extension curve is obtained by mechanical perturbing the structure of the molecule.

The chart progress of the force is obtained from adapted model of Hooke's Law, in most of the cases, the extension curve displays nonlinear behaviour, which can be described by the worm-like chain model (WLC) of entropic elasticity.

In Figure 17A are depicted two curves, where the red line represents theoretical curve obtain from the WLC model and blue dots form a graph of stretching and relaxing phase of the DNA measured by optical tweezers. A force in pN applied to DNA molecule by moving is plotted versus beads distance in μm . The overstretching transition occurs as we expected at about 65 pN [32] [2]. Overstretching of DNA at 65 pN is a melting transition Figure 17B. As we apply a force to increase the length of the molecule DNA, the dsDNA converts into ssDNA and this caused the plateau phase in curve. Our experiments showed an expected worm-like chain behavior, and overstretching transition at 65pN, which in summary means that our optical tweezers is properly set up and calibrated.

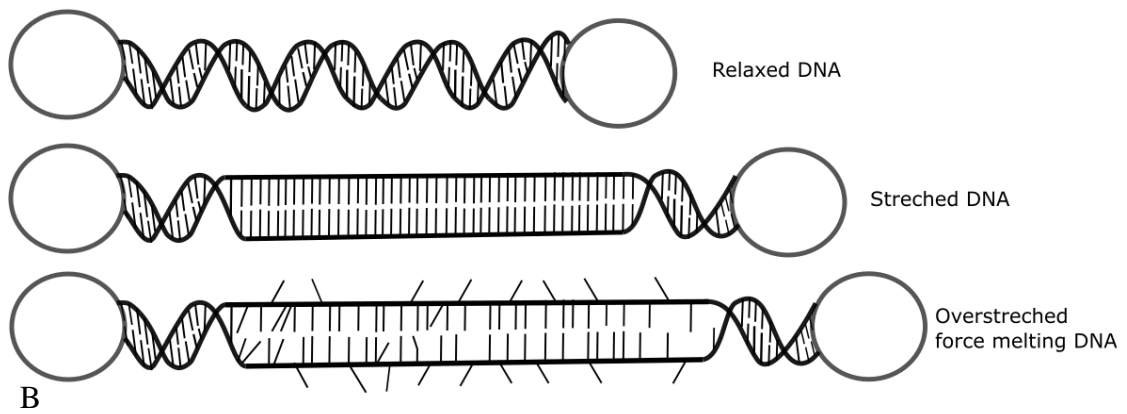
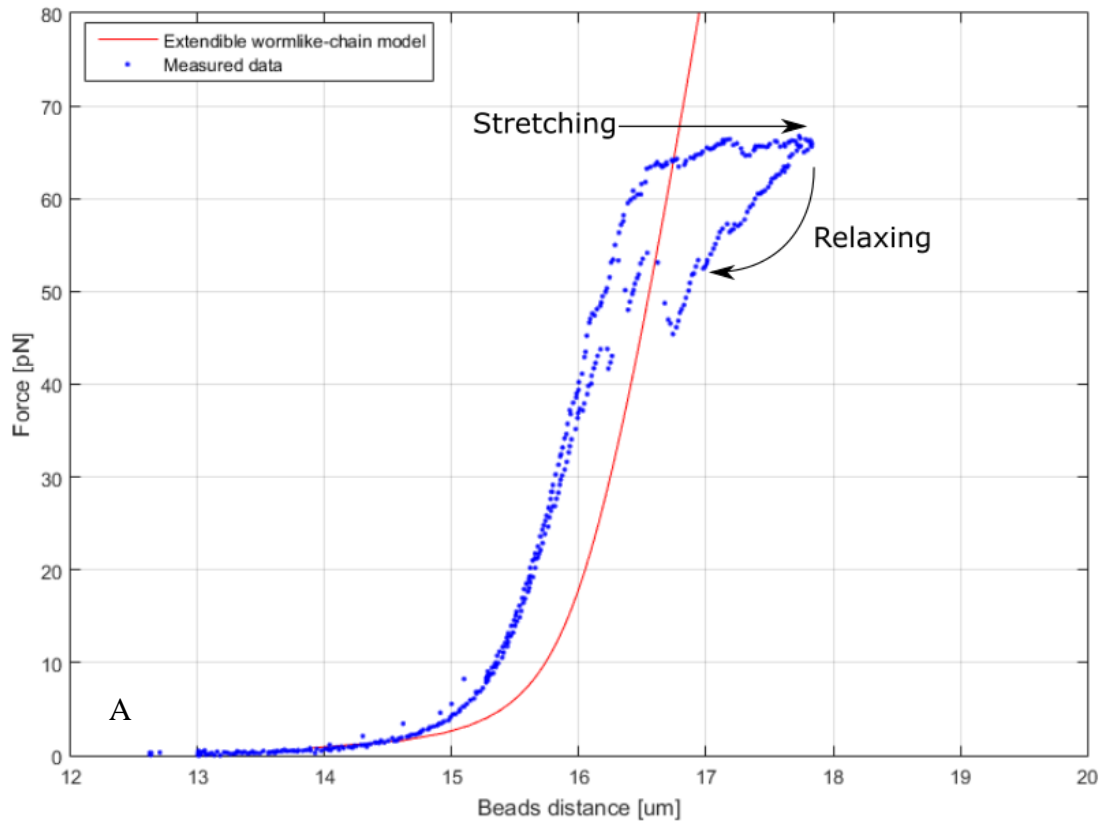


Figure 17: Force-distance curve of lambda DNA.

(A) The red line show us the extendible wormlike-chain WLC model calculated from Hook's law, using length of 55 nm, a contour length of 16,5 μm . It has a typical force-extension form of curve of a 3-3 attached DNA, with free 5 ends. At the inset). At 65 pN is well visible the overstretching transition, during which the dsDNA melting into ssDNA. (B) Schematic images of DNA tethered between two beads in relaxed state and after applying force by moving one of the beads. The overstretching plateau phase is caused by discontinuities in the phosphodiester backbone.

4.1.2 Binding of DNA intercalators

Binding of DNA intercalators was used for fluorescent imaging of DNA molecules and for calibration of the device for illuminating single molecules, such as kinesins. For experiment we chose SYTOX Orange fluorescent dye, usually used as a marker for dead cells. The SYTOX Orange dye was used in 10 nM concentration in PBS buffer, at first without any additional chemical solution.

Confocal imaging was provided by green laser at 543 nm wavelength. In Figure 18 is a confocal image of tethered DNA with visible single molecules of the fluorescent probe. With continual scanning of the DNA molecule one problem appeared, particularly that the molecule of the DNA was too fragile for scanning over longer time and after several seconds, the tethered molecule broke. For this reason, OxSc was added in PBS

In Figure 20 we can see, that the binding of the Sytox depends on the stretching - during the periods of relaxation of the DNA, only short binding events of single molecules of sytox are observed, whereas during the periods of extension longer binding events are observed. Figure 19 shows the histogram of fluorescence intensities of individual SYTOX binding events, such as shown in Figure 18. The intensity histogram has a nearly Gaussian profile. In combination with the fact that all observed SYTOX binding events bleached (or detached from DNA) in a single step, our results suggest that the single binding events correspond to single STOX molecules. We thus showed, that with our confocal microscopy system, it is possible to obtain a result from a single protein molecule.



Figure 18: Confocal image of dsDNA tethered between two beads

For imaging was used confocal microscopy with 543 nm wavelength. In the picture is captured tethered DNA between two beads (3.5 μm in diameter). The DNA molecule is visualized thanks to fluorescent dye Sytox Orange in 10 mM concentration.

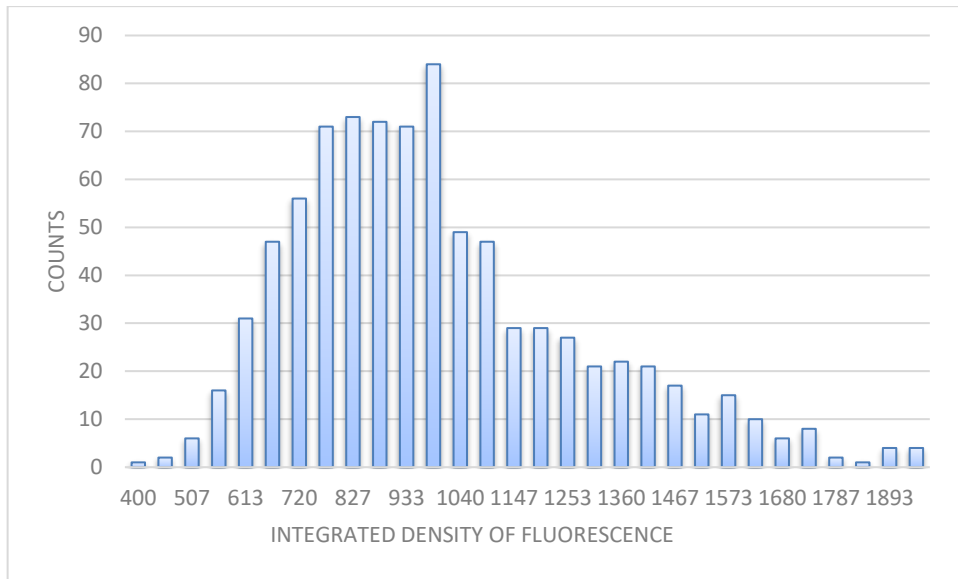


Figure 19: Gaussian distributions of fluorescent density

The histogram shows integrated intensity of fluorescence of individual Sytox Orange binding events to the MT (n = 850). Data as shown in Figure 18.

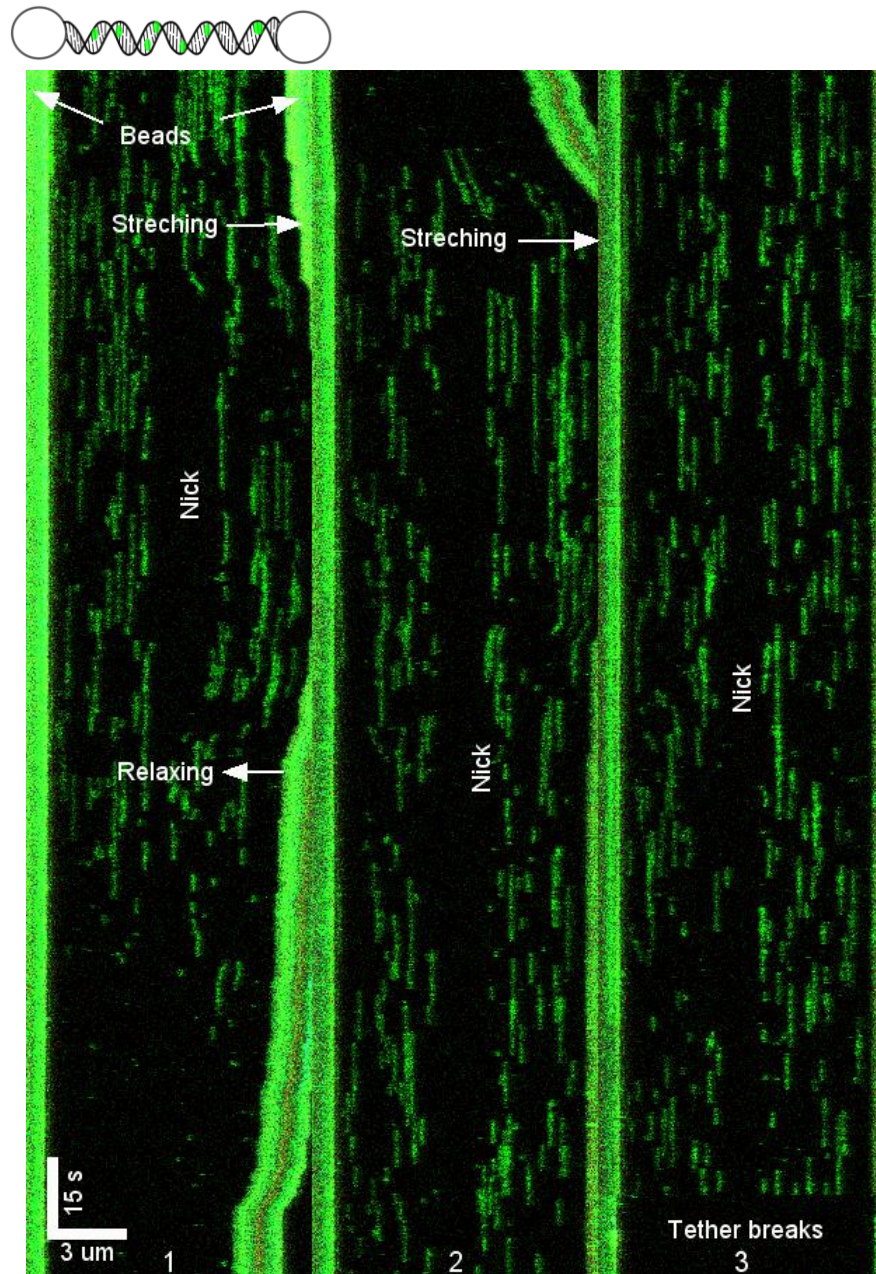


Figure 20: Kymographs of binding fluorescent dye Sytox Orange to DNA

Kymograph showing the force dependent binding dynamics of Sytox-Orange on DNA, the force is applied by moving the right bead and stretching the DNA. Green fluorescent stripes are records of the movement by $3.5\ \mu\text{m}$ polystyrene beads, white arrows indicate the stretching and relaxing phases of the DNA. Inside PBS buffer was placed oxygen scavenger – glucose oxidase (concentration $0.22\ \text{mg/ml}$), catalase (concentration $0.02\ \text{mg/ml}$) and glucose (concentration 20mM), which help us to make the DNA molecule more stable over time and record a long kymograph around 5 minutes long until the tether breaks. For illumination of the whole kymograph, one record was split into three independent images 1,2 and 3 proceeds from the top downwards. During the period of DNA relaxation, almost none binding is visible, compare to the stretching phase, where the binding is obvious. During the stretching phase, the area in the middle of the DNA is without any interaction with the Sytox Orange dye. It might be caused by presence of nick, a discontinuity in a dsDNA molecule, where there is no phosphodiester bond and no possible bounding of the fluorescent dye. In stretching curve, this area can be observed as the plateau phase.

4.2 Kinesin – 14 HSET experiments

The reason for previous proof-of-concept experiments was the preparation of the optical tweezers for the experiments focused on the microtubule-crosslinking by the motor protein kinesin-14, HSET.

4.2.1 TIRF experiment results

Coverslips were prepared according to the process explained in the Methods chapter. Briefly, we used glass flow chamber made of two small cover slips stuck together with parafilm. Each channel was coated with anti-biotin antibody, which has an affinity for biotinylated microtubules. Purified GFP-HSET kinesins crosslinked the immobilized microtubules with non-biotinylated microtubules, which were added later into the measurement chamber and the GFP-HSET-mediated interaction between the two microtubules was observed.

Similarly, to other kinesin-14 motors we observed that GFP-HSET in presence of ATP was sliding the two crosslinked microtubules relative to each other. In Figure 23 are captured several shots from the TIRF video at different times, on which the change of the position of the non-biotinylated microtubule is clearly visible. Our experiments revealed, that unlike other kinesin-14, the kinesin-14 HSET molecules have a special ability to decelerate the sliding of two microtubules when the microtubules start sliding apart, such that a stable overlap between the microtubules is maintained for tens of minutes, as is visible from the kymograph in Figure 23.

Quantification of the fluorescence intensity of GFP-HSET molecules in the overlap in experiments, such as presented in Figure 21, revealed that the GFP-HSET density in the overlap increases as the two microtubules slide apart. This observation suggests that GFP-HSET molecules are confined in the shortening overlap. Confinement of microtubule crosslinkers can lead to the generation of an entropic force, which acts in the direction of increasing the overlap lengths similarly to pressure generation by confined particles of gas [33].

We thus hypothesized that the observed deceleration of GFP-HSET driven sliding might be caused by an analogous entropic force generated by GFP-HSET molecules in the overlap. We thus designed the following experiments to test this hypothesis.

To answer the question, if GFP-HSET can generate entropic forces, we must uncouple the ATP-dependent GFP-HSET motor-generated force from the putative ATP-independent entropic force. The motor-domain of the kinesin, responsible for the ATP-dependent movement, must thus be inactivated. To achieve this, ADP was added into the measurement buffer instead of ATP. We then formed microtubule pairs as in the previous experiment and observed those microtubule pairs that were not overlapping with their full lengths, but only partially. The relative movement of partially overlapping microtubules would change the entropy of the crosslinkers bound between the microtubules as is visualized in Figure 22. The system has tendency to reach the maximal overlap with maximal possibilities for crosslinking. [34]

As seen on the Figure 24, we observed that partially overlapping microtubules crosslinked by GFP-HSET in presence of ADP were sliding in the direction increasing the overlap length, i.e. increasing the entropy of the system. We neither observed sliding of fully overlapping microtubule pairs nor did we observe sliding of partially overlapping microtubules in the direction decreasing the overlap length. These results suggest that GFP-HSET is capable of generating an entropic force independent of its ATP-ase activity acting always in the direction of increasing the overlap length.

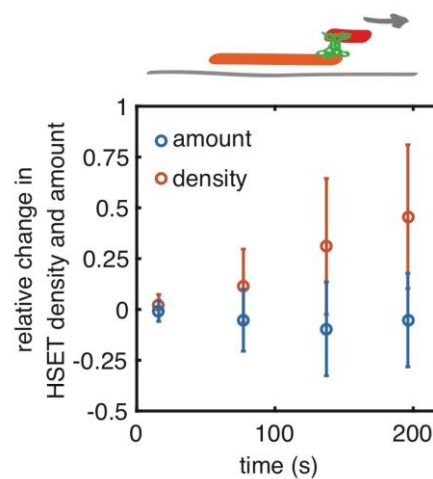


Figure 21 Increasing density of motor proteins in shortening overlaps.

The number of GFP-HSET molecules in the shortening overlaps remained approximately constant as the microtubules slid apart (time $t = 0$ corresponds to the moment, when microtubules started to separate), leading to progressive increase in GFP-HSET densities in the shortening overlaps. The data represent binned and averaged values (\pm SD; $n = 33$).

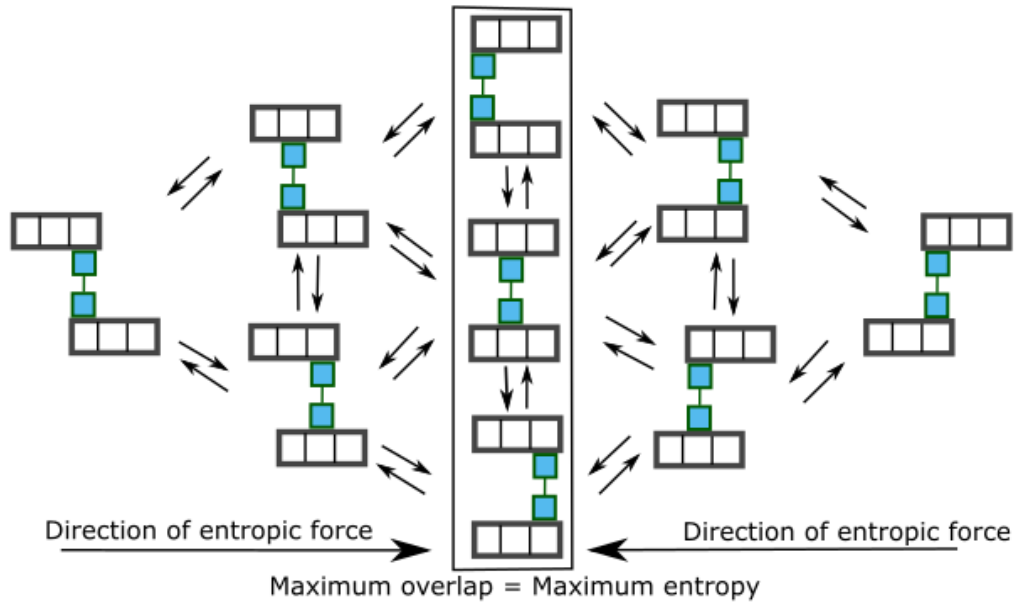


Figure 22 Schematic explanation of entropic force existence

As example are two microtubules of length with 3 binding sites crosslinked with 1 kinesin. The maximal overlap with 3 possible configurations, has also the maximal entropy. If the system partially overlapping, so the overlap has 2 or 1 possible configurations, there will be a decrease in entropy. The most probable state of the system is the one with the maximal entropy and the system creates a driving entropic expansion force to maximize the overlap. (Figure is taken over from [34])

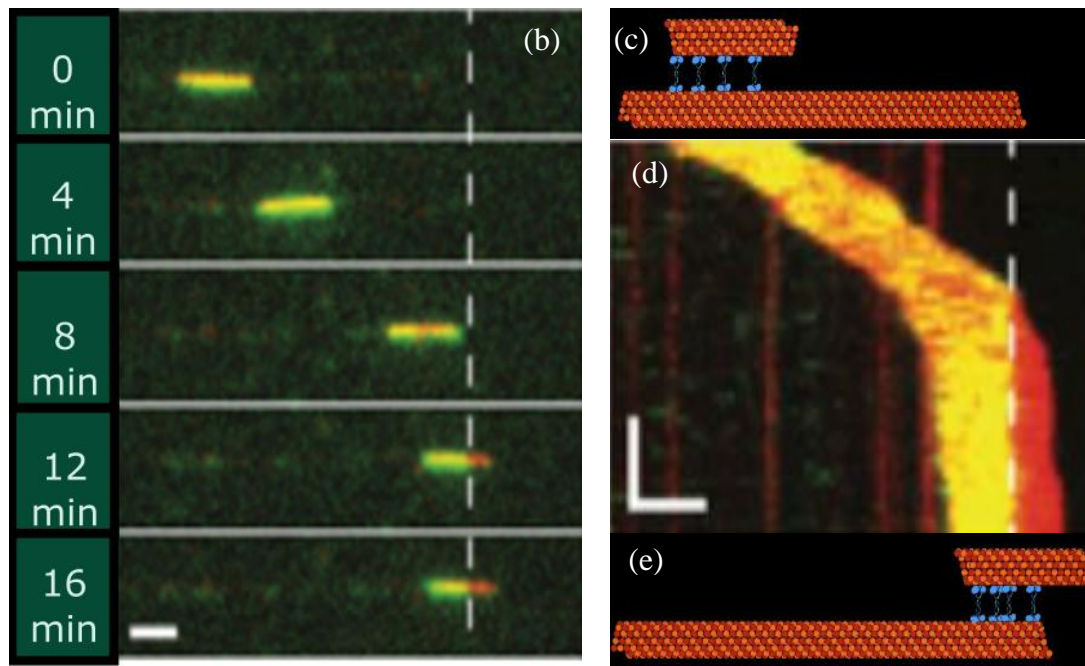
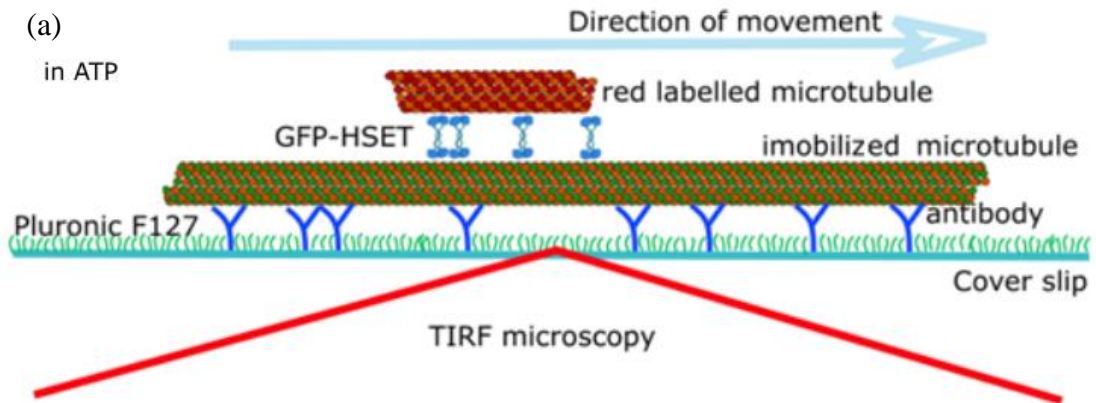


Figure 23 Sliding of two microtubules crosslinked with kinesin-14 HSET over each other with ATP.

a) Schematic image of GFP-HSET sliding of a shorter microtubule along a surface-immobilized microtubule. (b) Fluorescent image of long unlabeled microtubule immobilized on the surface of coverslip and shorter red Rhodamine labeled microtubule sliding over each other crosslinked by GFP-HSET at 1.5 nM concentration. (Dashed line indicated the end of the unlabeled microtubule) (c) visualization of full overlap (d) multichannel kymograph of how the shorter microtubule is sliding over the unlabeled one and generating entropic forces in opposite direction than movement of motor domain. (e) visualization of the stable overlap, formed after both microtubules reach their ends.

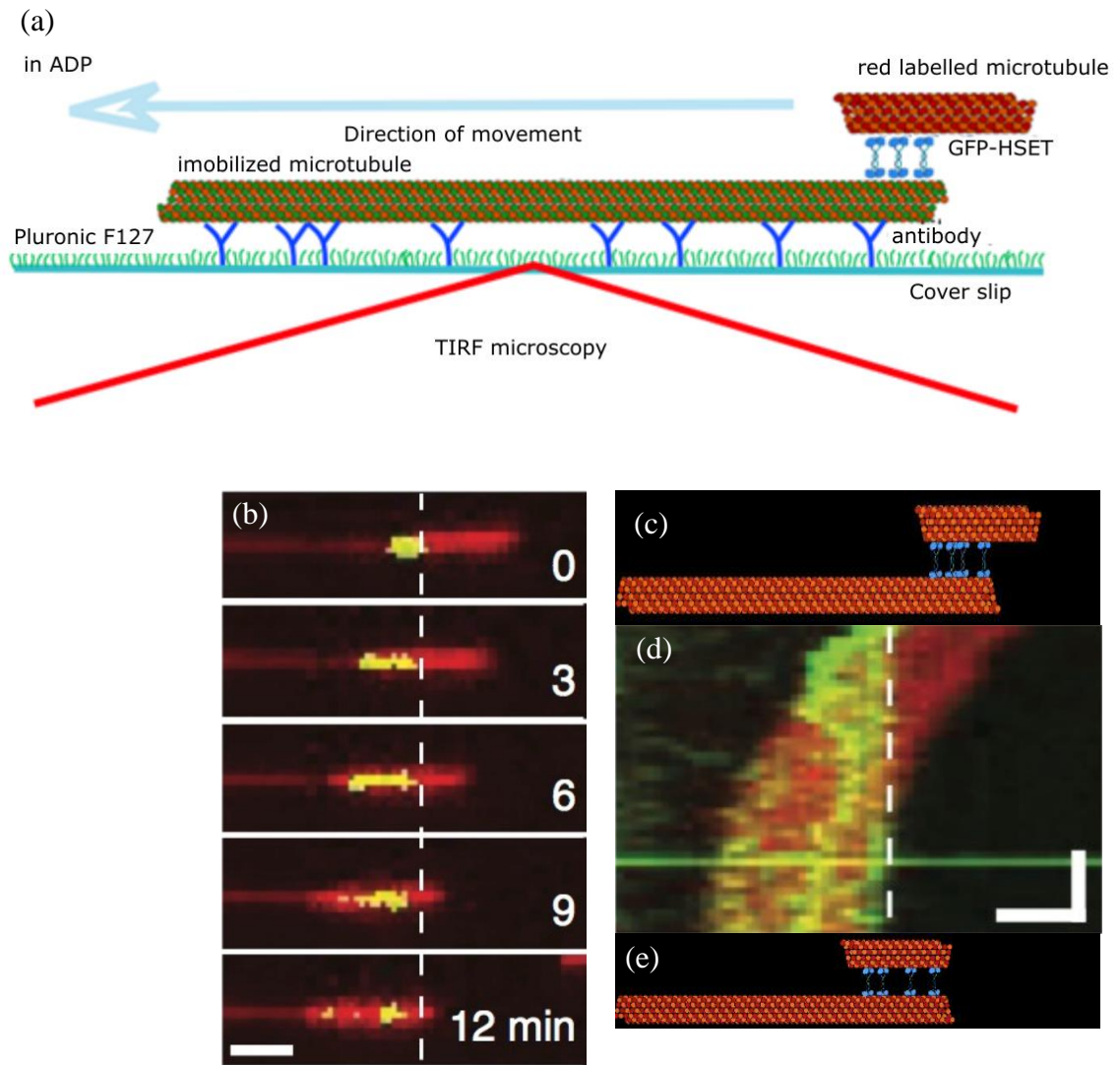


Figure 24 Return of two microtubules crosslinked with kinesin-14 HSET into maximal overlap in presence of ADP.

a) Schematic image of GFP-HSET sliding of a shorter microtubule along a surface-immobilized microtubule. (b) Fluorescent image of long microtubule immobilized on the surface of coverslip and shorter one sliding over each other crosslinked by GFP-HSET with ADP in solution (Dashed line indicated the end of the longer microtubule) (c) visualization of the stable overlap, formed after both microtubules reach their ends.) (d) multichannel kymograph of how the shorter microtubule is returning into the maximal overlap state with inactivated motor-domain. (e) visualization of full overlap

4.2.1 Optical tweezers experiment results

Lastly, we aimed to quantify the entropic force generated by HSET. The experiment was prepared using commercially available glass chip with flow cell inside. This glass chip can be repeatedly used, after cleaning procedure. It is possible to use it many times without any necessity to prepare coverslips by ourselves. The main advantage of this chip, is that over the whole length it has the same dimensions and during its movement, the sample, objective and condenser cannot be broken or damaged.

4.2.1.1 Force measurement

To measure the force two microtubules were attached to two beads (1.12 μm silica), held by two traps. The microtubules were then allowed to get crosslinked by GFP-HSET in the presence of ADP. The two microtubules were then pulled apart. The relative movement of the two microtubules along each other was generated by moving one of the two beads by the optical trap and according to in-build system the deflection of the bead inside trap was recalculated into force. During the force measurement, microtubules and GFP-HSET were visualized by confocal imaging using 488 nm and 647 nm excitation wavelengths.

In Figure 25 is a sequence of fluorescent images of the movement provided by optical tweezers, the overlap end is indicated by a white dashed line. We observed, that the kinesins form clusters and stick to the microtubules without any movement.

In Figure 26 is a force time-trace recorded during the confocal imaging. The movement of the bead driven by the optical trap was generated in steps of 200 nm, which are represented by the blue curve (23b), for each step there is a corresponding peak in the recorded force time-trace (23a), the applied force for each peak corresponds to ~ 15 pN. After each step, we allowed the system to reach the equilibrium before moving the trap further, which took on average 16.7 seconds. As the distance between beads grows and the length of the overlap shortens, the time to reach the equilibrium lengthens. The equilibrium force corresponds to the amplitude of the entropic force generated by GFP-HSET confined in the shortening overlap of the particular length.

In Figure 27 we can see, the force changing proportionally to increasing distance between beads and so shortening of the overlap. To measure the difference in the magnitude of the entropic force between two different lengths of the overlap (two different bead positions),

the two equilibrium force values were subtracted as visualized in Figure 28. We found that the force increased with decreasing overlap length and reaching values of about 19 pN, the force is obtained as difference between the initial equilibrium force before moving the trap and the final value of force just before the two microtubules separated.

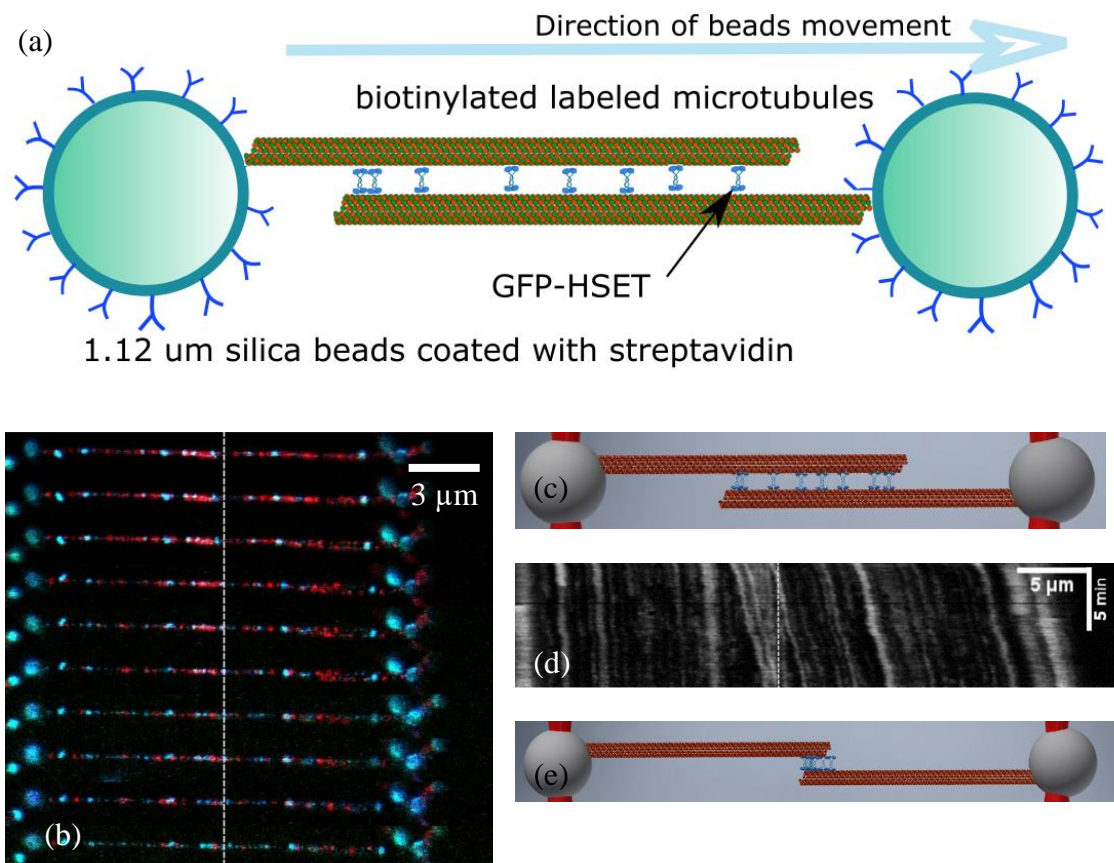


Figure 25: Image results from entropic force investigation

(a) In the schematic image is possible to see, how two coated microspheres serve as a mediator for manipulation with biotinylated microtubules crosslinked by GFP-HSET. (b) According to the video sequence from confocal fluorescent microscopy we can distinguish the end of the overlap (marked by white dashed line) and follow, how the kinesins motor density rises under the overlap. (c,e) animation of the starting position with partial overlap and the position just before separation. (d) kymograph of the movement of the kinesins along the microtubule, as the force is applied on them by trap moving. It might be visible, that the measurement is not clear because of kinesins clusters all along both microtubules.

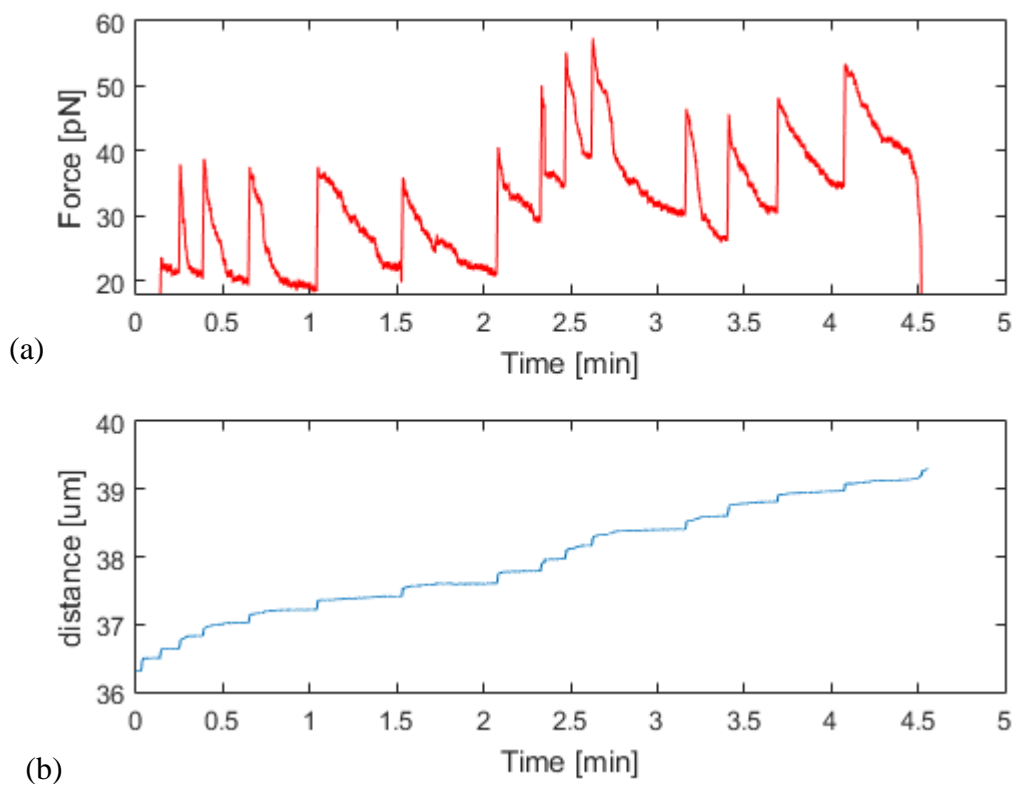


Figure 26: Resulting force curve recorded by stepping movement of one of the traps. The trap was moved in steps with constant velocity $0.1 \mu\text{m/s}$ in $0.2 \mu\text{m}$ steps. The upper graph (a) shows us the force change in time, each red peak respond to one step. In the lower graph (b) is visualized distance change in time. The entropic force is obtained as a difference between the equilibrium force before breaking and the initial force $\sim 19 \text{ pN}$.

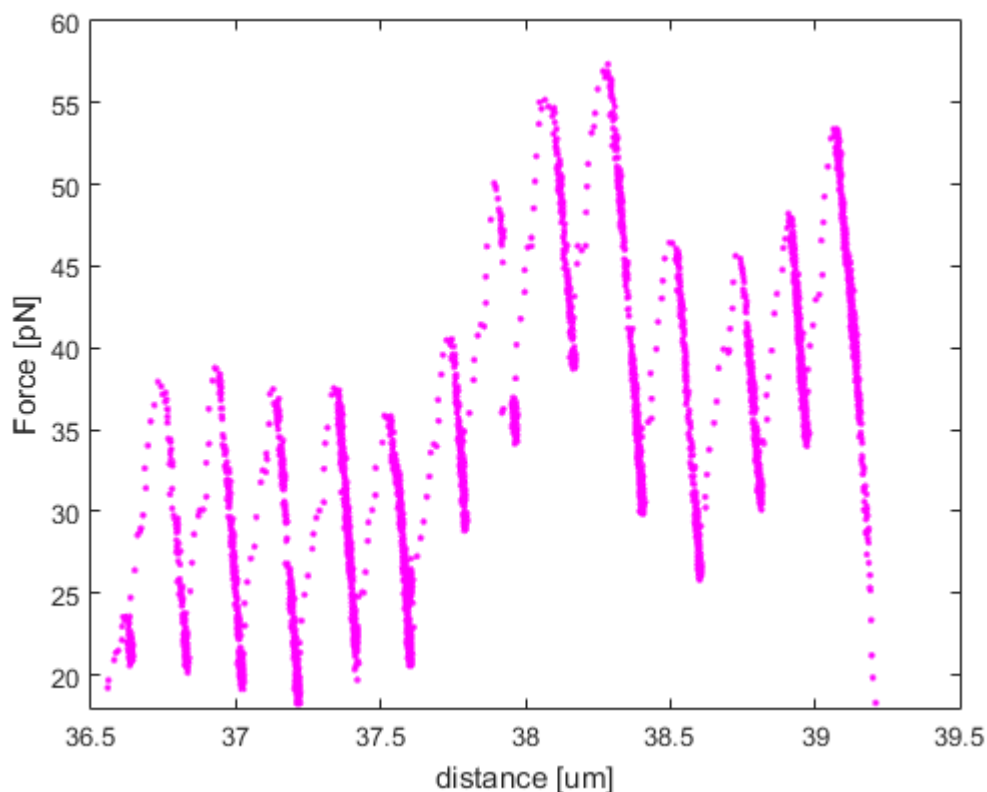


Figure 27: Force distance curve for previous result.

The time traces were further analyzed and converted into force-distance curves using an in-build software. We can observe small drifting between each step, which is supposed to grow with decreasing overlap (increasing distance between beads). For the area around 36.5 μm and 37.5 μm the offset is relative stable around zero, around 38 μm the offset force is rapidly growing, but after few steps decreases again. In the area between 38.5 μm and 39 μm the offset force is increasing until the overlap is fully separated and falls to zero. In correlation with image sequence, we observe several things, which might be the reason for this force drift. The most probable reason is presence of clusters kinesins, which might have blocked the movement.

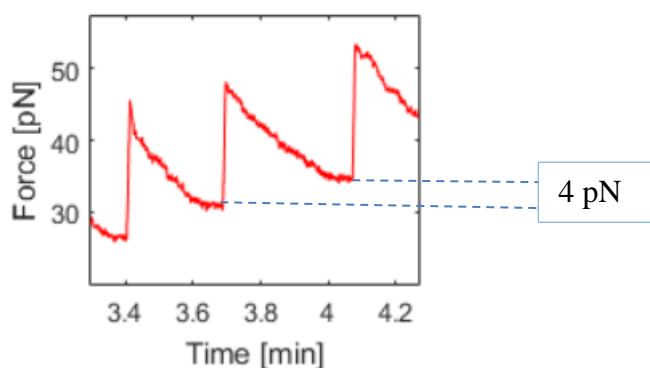


Figure 28: Cut out from force/time graph showing offset force.

For each step was applied force around 15 pN, with increasing density of motors, the settling time grows. The change in the entropic force between the two steps shown in the figure is around 4 pN.

5 Discussion

5.1 DNA Experiment

My goal of this measurement was to prove, that the optical tweezers are well set up and capable of measuring forces with pN resolution and simultaneously visualizing single fluorescent molecules and are therefore suitable for use in experiments on cytoskeletal structures. For the actual experiment, we used lambda phage DNA (λ DNA) of contour length of 16.5 μm (48.5 kbp).

According to graph showing a stretching of a single molecule in Figure 17, it is possible to say, that at low level of extension, there are little changes visible in the measured force. After stretching the DNA further, the nucleotides start to respond similarly as elastic polymer and the force increases rapidly. This part of the curve responds similarly to the worm-like chain (WLC) model, which is used in polymer physics to describe the behaviour of semi-flexible polymers. Once the force reaches level around 65 pN, we can clearly see the overstretching phase. This experiment matches the published results [2] very well showing that force measurement on our optical tweezers is well set up and that the system is capable of quantitative force measurements.

For the single molecule visualization, we used DNA intercalating fluorescent dye SYTOX Orange for its several advantages. It binds to DNA rapidly in a manner of few seconds, based on high affinity the fluorescent dye shows for DNA molecules. It has a good signal-to-noise ratio for low concentration and it is known to be possible to be visualized at a single molecule level with confocal microscopy. Furthermore, the intercalator does not affect DNA mechanical properties and photobleaching rate is quite low. [31]

We showed that we were able to detect single SYTOX molecules and that with higher applied force on the molecule of DNA, SYTOX seems to bind with higher affinity to DNA and the dwell time of SYTOX on the DNA strand increases. For the single molecule imaging and force measurement, the stability of the bio-polymer structure in time is crucial. In our initial experiments, the problem with fragility of DNA appeared - the DNA would rupture after ~ 15 seconds. The issue was solved by the addition of OxSc into solution reducing the reactive oxygen species from solution. This also reduced the bleaching of the molecules of Sytox Orange. We thus used the OxSc also in our further

experiments with cytoskeletal structures. In summary, our proof of concept experiments using single DNA molecule as a model system showed that the system is well set up and capable of quantitative force measurements simultaneously with single molecule imaging.

5.2 Kinesin – 14 HSET Experiments

5.2.1 TIRF microscopy experiment

We showed that microtubules cross-linked by HSET slide over each other with constant velocity, until the overlap decreases to the critical point. As the microtubules start separating, the velocity of the sliding decelerates, until it forms a stable overlap for dozens of minutes. During this process, the density of HSET molecules in the overlap increases. One reason for this could be that the diminishing motor protein force might be due to the accumulation of the proteins together – leading to an increase in the collective frictional force or the decrease of the motor driving force by for example steric hindrance between the motors.

Our second hypothesis, was that the deceleration is caused by entropic forces generated by the HSET molecules confined in the overlap and acting against the motor driving force. Example of an entropic force, might be a gas expansion of compressed volume inside syringe (Figure 29). It represents a system, where particles under external load, reduce their entropy as the total number of microscopic states decreases. The entropic forces arise from the spontaneous relaxation into the maximal gas volume once the external load is removed, which is the state with the maximal entropy. Similar mechanism has been observed for diffusible microtubule crosslinkers [33].

Our initial experiment with two partially overlapping microtubules crosslinked by HSET in the presence of ADP showed that the two microtubules slide along each other such that the overlap length increases. As the ATP-dependent motor activity is disabled in this case and the microtubules always slide in the direction of increased overlap it is very like that the HSET molecules actually do generate entropic forces in the microtubule overlap. We thus designed the following optical trap experiment to measure the entropic force directly.

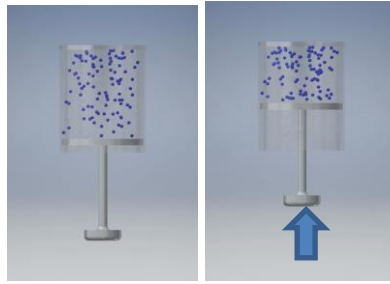


Figure 29: Particles of gas inside the cylindrical volume.

Our idea is that HSET confined in a shortening overlap, is analogous to the particles of gas confined in a finite volume, such as a cylinder with a piston. External load pressing the piston is analogous to the ATP-dependent motor force shortening the microtubule overlap. Pressure generated by the gas inside of the cylinder would be analogous to the HSET ATP-independent entropic force.

5.2.2 Optical Tweezers force measurement

The optical tweezers were used for this experiment in order to measure the entropic forces generated by HSET in the microtubule overlap. For the experiment, we chose the two beads setup, where one end of each microtubule is bound to one of the beads and the opposite microtubule ends were crosslinked by the GFP-HSET.

We measured this force in a buffer containing ADP instead of ATP, which inactivated the motor part of the kinesin. The measurement was conducted by moving one of the beads relative to the other on, thus moving the two microtubules along each other such that the overlap between them decreased. We performed the measurement of this force by displacing one of the beads in defined steps and then waiting for the system to reach an equilibrium, in other words until the kinesins in the overlap reorganized themselves. In this moment, the force detected should correspond to the entropic force generated by the motors in the overlap. We observed that as the two microtubules were slid apart (and the overlap length decreased), this equilibrium force value increased reaching up to ~ 19 pN. The increase in the force is expected, and is analogous to the pressure increasing with decreasing volume. The magnitude of the force is surprisingly high compared to other entropic cytoskeletal systems [33]. This might be due to several technical issues that we were facing during the experiments (see below for details) and the experiments will have to be repeated in future to ensure their validity.

5.2.2.1 Binding issues

During the experiment, the binding of microtubules to the beads appeared as the most complicated issue. For the experimental set up I tried to use polystyrene beads of $4.5\ \mu\text{m}$ in diameter coated with streptavidin. Their advantage is that they are visible in the fluorescence imaging channel, which helped us to correlate the fluorescent image with the bright field image.

After several experiments, we discovered, that the material of the beads might not be suitable for cytoskeletal structures. We observed that the microtubules were detaching from the beads at forces around 7-12 pN, which was too low for the measurement of the entropic forces.

According to the confocal video, which is in cut form visualized in Figure 30, one problem might have been the beads size. The large $4.5\ \mu\text{m}$ beads clearly induced mechanical deformation to the microtubule lattice during sliding apart. We replaced these beads with smaller, $1\ \mu\text{m}$ diameter polystyrene beads. The smaller size of polystyrene beads reduced mechanical deformation caused by the movement, but the tearing of the microtubules from the beads was still present. The problem was finally solved by replacing the material of beads. For the final experiments, we used silica beads with diameter of $1.12\ \mu\text{m}$.

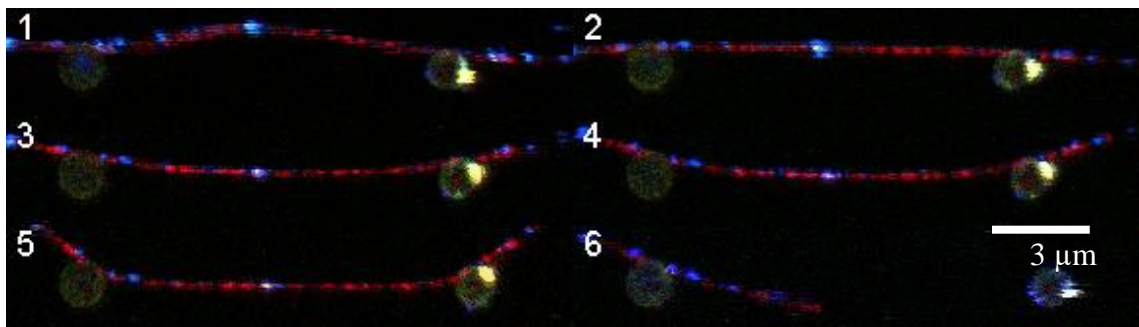


Figure 30: Mechanical deformation of microtubule

For the experiment were used GMPCPP biotinylated Alexa 647 labeled microtubules and $2.5\ \mu\text{m}$ polystyrene beads. From the image sequence is visible, that because of the rigid structure and larger diameter of beads, the microtubules are under mechanical deformation, which may cause the breaking and tearing apart from beads.

It is possible, that the problem was due to undesirable production of reactive oxygen species close to the bead surface, because of the material and this could cause the breakage of microtubule near to the bead's surface. The disadvantage of the silica beads is that in the bright field imaging, where we can see the beads trapped inside the light

beam, they display only a very low contrast compared to the surrounding area. It is thus hard to observe such small objects and to be sure, that only one bead is present inside the trap. In Figure 31 are two images from the bright field microscopy used for visualization of trapped beads.

One more disadvantage of the silica beads is, that they are quite heavy and usually sink to the bottom of the glass chip, where they stick to the surface and form a blockade of the flow cell. On the other side, it solved most of our issues. It was possible to image both of the bound microtubules, cross-linked together with HSET kinesin and measure the produced force.

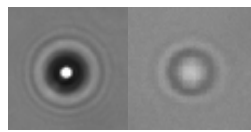


Figure 31: Comparison of two trapped beads visualized in bright field.

On the left, there are a 4.5 μm in diameter polystyrene bead (Spherotech) and in the right image, there is a silica bead 1.12 μm in diameter (Spherotech). In these two images, it can be easily seen, why the polystyrene beads are more usual for the force investigation. For the user, less contrast is a disadvantage.

5.2.2.2 Factors affecting the measurement

We measured HSET entropic forces reaching up to ~ 19 pN, which is a rather high value. Also during the measurement, when we were sliding the microtubules apart with the optical tweezers, we didn't observe a monotonous increase of the entropic force, which we would expect. Rather we observed intermittent periods of increase and decrease (see Figure 26 and Figure 27). We argue that this might be due to the quality of the protein preparation. According to correlation of time and image, I have observed, that the force measurement might be influenced by clusters of kinesins binding to the microtubules (see Figure 25). These clusters most likely do not represent a physiological state of the motor, but are the result of an unspecific aggregation process. For this reason, more investigation has to be made to prove, that the entropic force is present and to estimate the magnitude of the force.

The main factor influencing the protein clustering is temperature. The optimal temperature for microtubules is around 25°C . On the other hand, to maintain the stability of kinesin molecules, the temperature needs to be quite lower as they prefer to stay near zero $^{\circ}\text{C}$. This need for two largely different temperatures present in the medium,

presented a considerable challenge for the tweezers experiment, and could possibly be one of the present obstacles for proper measurement.

Another of the most problematic parts of this experiment, was the crosslinking of the microtubules, because it is almost impossible to catch only one microtubule on each bead at given time and try to rotate them in the opposite direction, to do so for the possibility of the crosslinking. The idea for solving this problematic part might be to use four traps set up and manipulate with more beads.

6 Conclusions

In this work, I aimed to analyse mechanical properties of biopolymers. The two biopolymers chosen for this work represent two very different biological structures. On one hand a single DNA filament, a very flexible structure and on the other hand an assembly of cytoskeletal filaments, microtubules, in comparison to DNA a very stiff structure. DNA experiment was realized mostly to perform proof of concept measurement, serving as a calibration and to prepare the device for subsequent cytoskeletal experiments. We showed that the DNA is flexible molecule following the worm-like chain model and its overstretching is achieved when force of approximately 65 pN is applied. Experiment with Sytox Orange helped us to test the resolution of fluorescent imaging. We showed, that with confocal imaging it is possible to obtain a single molecule resolution.

The investigation of kinesin-14, HSET brought us some new information about how this protein works to promote the assembly of microtubules into higher order structures, namely stable microtubule bundles. Using TIRF microscopy we discovered that the behaviour of this type of kinesins is atypical to other kinesin-14 family members. With reduction of the overlap, the HSET sliding velocity decelerates and after reaching equilibrium, we can observe a stable overlap. Our experiments suggest that this deceleration is a consequence of entropic force. My results show, that it is possible to measure the entropic forces using optical tweezers, but with the final result, the quantification of the force, we cannot be absolutely certain due to technical issues that will require further work to solve.

We were able to observe similar phenomenon in both bio-polymeric structures that we investigated, that is entropy driven contraction of the structure. On one hand, it was the entropic elasticity of a single DNA biopolymer, resisting the external load applied by the optical tweezers during the DNA stretching experiment. On the other hand, it was the higher order biopolymer assembly comprising microtubules crosslinked by HSET molecular motors, tending to entropically contract to the state of maximal length of the overlap between the filaments, which resisted the external load applied on the filaments by the optical tweezers during the microtubule sliding experiment. Our results thus in combination point to analogous principles governing the mechanical properties of

biopolymers form single flexible polymeric chains to stiff higher order polymeric assemblies.

References

- [1] CAI, S., L. WEAVER, S. EMS-MCCLUNG a C. WALCZAK. Kinesin-14 Family Proteins HSET/XCTK2 Control Spindle Length by Cross-Linking and Sliding Microtubules. *Molecular Biology of the Cell* [online]. 2009, **20**(5), 1348-1359 [cit. 2017-03-26]. DOI: 10.1091/mbc.E08-09-0971. ISSN 10591524. Available from: <http://www.molbiolcell.org/cgi/doi/10.1091/mbc.E08-09-0971>
- [2] VAN MAMEREN, J., P. GROSS, G. FARGE, P. HOOIJMAN, M. MODESTI, M. FALKENBERG, G. J. L. WUITE a E. J. G. PETERMAN. Unraveling the structure of DNA during overstretching by using multicolor, single-molecule fluorescence imaging. *Proceedings of the National Academy of Sciences* [online]. 2009, **106**(43), 18231-18236 [cit. 2017-05-16]. DOI: 10.1073/pnas.0904322106. ISSN 00278424. Available from: <http://www.pnas.org/cgi/doi/10.1073/pnas.0904322106>
- [3] ALBERTS, Bruce. *Essential cell biology*. 3rd ed. New York: Garland Science, 2009. ISBN 9780815341307.
- [4] ALBERTS, Bruce. *Molecular biology of the cell*. Sixth edition. b.r. ISBN 9780815344643.
- [5] TUSZYNSKI, J. *Molecular and cellular biophysics*. Boca Raton: Chapman & Hall/CRC, 2008. ISBN 9781584886754.
- [6] NABI, Ivan. *Cellular domains*. Hoboken, N.J.: Wiley-Blackwell, 2011. ISBN 9781118015759.
- [7] SCHLIWA, Manfred a Günther WOEHLKE. Molecular motors. *Nature* [online]. 2003, **422**(6933), 759-765 [cit. 2017-03-26]. DOI: 10.1038/nature01601. ISSN 00280836. Available from: <http://www.nature.com/doi/10.1038/nature01601>
- [8] MARX, A., J. MÜLLER a E. MANDELKOW. *The structure of microtubule motor proteins* [online]. b.r., s. 299 [cit. 2017-04-09]. DOI: 10.1016/S0065-3233(04)71008-6. Available from: <http://linkinghub.elsevier.com/retrieve/pii/S0065323304710086>
- [9] ENDOW, Sharyn a Douglas BARKER. Processive and Nonprocessive Models of Kinesin Movement. *Annual Review of Physiology* [online]. 2003, **65**(1), 161-175

- [cit. 2017-05-02]. DOI: 10.1146/annurev.physiol.65.092101.142550. ISSN 00664278.
- [10] RATH, Oliver a Frank KOZIELSKI. Kinesins and cancer. *Nature Reviews Cancer* [online]. 2012, **12**(8), 527-539 [cit. 2017-04-09]. DOI: 10.1038/nrc3310. ISSN 1474175x. Available from: <http://www.nature.com/doifinder/10.1038/nrc3310>
- [11] KRATKY, O. a G. POROD. Röntgenuntersuchung gelöster Fadenmoleküle. *Recueil des Travaux Chimiques des Pays-Bas* [online]. 1949, **68**(12), 1106-1122 [cit. 2017-05-18]. DOI: 10.1002/recl.19490681203. ISSN 01650513. Available from: <http://doi.wiley.com/10.1002/recl.19490681203>
- [12] FUNAYAMA, Ryoto, Yoshio NAKAHARA, Shinpei KADO, Mutsuo TANAKA a Keiichi KIMURA. A single-molecule force-spectroscopic study on stabilization of G-quadruplex DNA by a telomerase inhibitor. *The Analyst* [online]. 2014, **139**(16), 4037- [cit. 2017-05-11]. DOI: 10.1039/C4AN00439F. ISSN 00032654. Available from: <http://xlink.rsc.org/?DOI=C4AN00439F>
- [13] ASHKIN, A. Acceleration and Trapping of Particles by Radiation Pressure. *Physical Review Letters* [online]. 1970, 24(4), 156-159 [cit. 2017-05-18]. DOI: 10.1103/PhysRevLett.24.156. ISSN 0031-9007. Available from: <https://link.aps.org/doi/10.1103/PhysRevLett.24.156>
- [14] VAN MAMEREN, Joost, Gijts J. L. WUITE a Iddo HELLER. Introduction to Optical Tweezers: Background, System Designs, and Commercial Solutions [online]. s. 1 [cit. 2017-05-18]. DOI: 10.1007/978-1-61779-282-3_1. Available from: http://link.springer.com/10.1007/978-1-61779-282-3_1
- [15] ASHKIN, A., J. M. DZIEDZIC, J. E. BJORKHOLM a Steven CHU. Observation of a single-beam gradient force optical trap for dielectric particles. *Optics Letters* [online]. 1986, 11(5), 288- [cit. 2017-05-18]. DOI: 10.1364/OL.11.000288. ISSN 01469592. Available from: <https://www.osapublishing.org/abstract.cfm?URI=ol-11-5-288>
- [16] HECHT, Eugene. *Optics*. 4th ed. Reading, Mass.: Addison-Wesley, 2002. ISBN 9780805385663.

- [17] NIEMINEN, Timo, Gregor KNÖNER, Norman HECKENBERG a Halina RUBINSZTEIN-DUNLOP. *Physics of Optical Tweezers* [online]. b.r., s. 207 [cit. 2017-04-03]. DOI: 10.1016/S0091-679X(06)82006-6. Available from: <http://linkinghub.elsevier.com/retrieve/pii/S0091679X06820066>
- [18] ASHKIN, A. Forces of a single-beam gradient laser trap on a dielectric sphere in the ray optics regime. *Biophysical Journal* [online]. 1992, **61**(2), 569-582 [cit. 2017-02-22]. DOI: 10.1016/S0006-3495(92)81860-X. ISSN 00063495. Available from: <http://linkinghub.elsevier.com/retrieve/pii/S000634959281860X>
- [19] ASHKIN, A., J. DZIEDZIC, J. BJORKHOLM a Steven CHU. Observation of a single-beam gradient force optical trap for dielectric particles. *Optics Letters* [online]. 1986, **11**(5), 288- [cit. 2017-02-22]. DOI: 10.1364/OL.11.000288. ISSN 01469592. Available from: <https://www.osapublishing.org/abstract.cfm?URI=ol-11-5-288>
- [20] NIR, Guy, Moshe LINDNER a Yuval GARINI. Protein-DNA Interactions Studies with Single Tethered Molecule Techniques. *Protein Interactions* [online]. InTech, 2012 [cit. 2017-03-13]. DOI: 10.5772/38416. ISBN 9789535102441. Available from: <http://www.intechopen.com/books/protein-interactions/protein-dna-interactions-studies-with-single-tethered-molecule-techniques>
- [21] BROUWER, Ineke, Graeme KING, Iddo HELLER, Andreas BIEBRICHER, Erwin PETERMAN a Gijis WUITE. *Probing DNA–DNA Interactions with a Combination of Quadruple-Trap Optical Tweezers and Microfluidics* [online]. b.r., s. 275 [cit. 2017-05-14]. DOI: 10.1007/978-1-4939-6421-5_10. Available from: http://link.springer.com/10.1007/978-1-4939-6421-5_10
- [22] WILLIAMS, Mark. *Optical Tweezers: Measuring Piconewton Forces, in Single Molecule Technique* [online]. 2002 [cit. 2017-05-16]. Available from: <http://www.biophysics.org/Portals/1/PDFs/Education/williams.pdf>
- [23] NEUMAN, Keir a Steven BLOCK. Optical trapping. *Review of Scientific Instruments* [online]. 2004, **75**(9), 2787-2809 [cit. 2017-04-18]. DOI: 10.1063/1.1785844. ISSN 00346748. Available from: <http://aip.scitation.org/doi/10.1063/1.1785844>

- [24] GITTES, Frederick a Christoph SCHMIDT. Interference model for back-focal-plane displacement detection in optical tweezers. *Optics Letters* [online]. 1998, **23**(1), 7- [cit. 2017-05-13]. DOI: 10.1364/OL.23.000007. ISSN 01469592. Available from: <https://www.osapublishing.org/abstract.cfm?URI=ol-23-1-7>
- [25] ARNE GENNERICH. *Optical tweezers: Methods and Protocols*. Springer Science+Business Media New York: Humana Press, 2017, XII, 555. 1. ISBN 9781493964192. DOI: 10.1007/978-1-4939-6421-5.
- [26] BERG-SØRENSEN, Kirstine a Henrik FLYVBJERG. Power spectrum analysis for optical tweezers. *Review of Scientific Instruments* [online]. 2004, **75**(3), 594-612 [cit. 2017-05-13]. DOI: 10.1063/1.1645654. ISSN 00346748. Available from: <http://aip.scitation.org/doi/10.1063/1.1645654>
- [27] MURPHY, Douglas. *Fundamentals of light microscopy and electronic imaging*. New York: Wiley-Liss, 2001. ISBN 047125391x.
- [28] INOUÉ, Shinya. Foundations of Confocal Scanned Imaging in Light Microscopy. *Handbook of Biological Confocal Microscopy* [online]. Boston, MA: Springer US, 1995, s. 1 [cit. 2017-03-13]. DOI: 10.1007/978-1-4615-7133-9_1. ISBN 9781461571353. Available from: http://link.springer.com/10.1007/978-1-4615-7133-9_1
- [29] FISH, Kenneth. Total Internal Reflection Fluorescence (TIRF) Microscopy. *Current Protocols in Cytometry* [online]. Hoboken, NJ, USA: John Wiley & Sons, 2001 [cit. 2017-05-12]. DOI: 10.1002/0471142956.cy1218s50. ISBN 0471142956. Available from: <http://doi.wiley.com/10.1002/0471142956.cy1218s50>
- [30] Fluorescence SpectraViewer. *Thermo Fisher Scientific* [online]. 2017 [cit. 2017-05-11]. Available from: <https://www.thermofisher.com/cz/en/home/life-science/cell-analysis/labeling-chemistry/fluorescence-spectraviewer.html?ICID=svtool&UID>
- [31] THAKUR, Shreyasi, Diego CATTONI a Marcelo NÖLLMANN. The fluorescence properties and binding mechanism of SYTOX green, a bright, low photo-damage DNA intercalating agent. *European Biophysics Journal* [online]. 2015, **44**(5), 337-348 [cit. 2017-05-16]. DOI: 10.1007/s00249-015-1027-8. ISSN 01757571. Available from: <http://link.springer.com/10.1007/s00249-015-1027-8>

- [32] HELLER, Iddo, Gerrit SITTERS, Onno BROEKMANS et al. STED nanoscopy combined with optical tweezers reveals protein dynamics on densely covered DNA. *Nature Methods*. 2013, **10**(9), 910-916. DOI: 10.1038/nmeth.2599. ISSN 1548-7091. Available from: <http://www.nature.com/doifinder/10.1038/nmeth.2599>
- [33] LANSKY, Zdenek, Marcus BRAUN, Annemarie LÜDECKE, Michael SCHLIERF, Pieter Rein TEN WOLDE, Marcel E. JANSON a Stefan DIEZ. Diffusible Crosslinkers Generate Directed Forces in Microtubule Networks. *Cell* [online]. 2015, **160**(6), 1159-1168 [cit. 2017-05-16]. DOI: 10.1016/j.cell.2015.01.051. ISSN 00928674. Available from: <http://linkinghub.elsevier.com/retrieve/pii/S0092867415001294>
- [34] ODDE, David J. Mitosis, Diffusible Crosslinkers, and the Ideal Gas Law. *Cell* [online]. 2015, **160**(6), 1041-1043 [cit. 2017-05-16]. DOI: 10.1016/j.cell.2015.02.048. ISSN 00928674. Available from: <http://linkinghub.elsevier.com/retrieve/pii/S0092867415002494>
- [35] BOUCHIAT, C., M.D. WANG, J.-F. ALLEMAND, T. STRICK, S.M. BLOCK a V. CROQUETTE. Estimating the Persistence Length of a Worm-Like Chain Molecule from Force-Extension Measurements. *Biophysical Journal* [online]. 1999, **76**(1), 409-413 [cit. 2017-05-11]. DOI: 10.1016/S0006-3495(99)77207-3. ISSN 00063495. Available from: <http://linkinghub.elsevier.com/retrieve/pii/S0006349599772073>

List of Attachments

Attachment 1: Motility Buffer for HSET kinesin	69
Attachment 2: Polymerize GMPCPP-stabilized and double-stabilized microtubules....	70
Attachment 3: Full matlab code – Correlation of curve with image	71
Attachment 4: Full matlab code – Correlation of image with curve	73
Attachment 5: CD	75

Attachment 1: Motility Buffer for HSET kinesin

Table 1: Reagents of motility buffer

Volume	Reagent	Stock	Final Concentration
832.5 μ l	HEPES buffer	1x	1x
37.5 μ l	KCl	2 M	75 mM
10 μ l	Taxol	1 mM	10 μ M
50 μ l	Casein	10 mg/ml	0.5 mg/ml
10 μ l	Tween20	10% BRB80	in 0.1 %
10 μ l	ADP/ATP	80 mM	0.8 mM
10 μ l	DTT	1 M	10mM
10 μ l	D-Glucose	2 M	20 mM
10 μ l	Glucose oxidase	22.4 mg/ml	0.22 mg/ml
10 μ l	Catalase	2 mg/ml	0.02 mg/ml
10 μ l	Hexokinase	-	-

Mix all reagents on ice and for 30 minutes leave in degasser. Hexokinase, glucose oxidase and catalase add just before the experiment, it has to be fresh. Hexokinase and ADP are added in case, that the assay without motor movement is provided.

Attachment 2: Polymerize GMPCPP-stabilized and double-stabilized microtubules

Table 2: Reagents for polymerization of MTs with GMPCPP

Volume	Reagent	Stock	Final
5 μ l	RTU tubulin	4 mg/ml (40 μ M)	2 μ M
64 μ l	BRB80	1x	
10 μ l	GMPCPP	10 mM	1 mM
1 μ l	MgCl ₂	100 mM	1 mM

1. Mix reagents on ice and incubate 5 min on ice.
2. Incubate at least two hours at 37 °C.
3. Spin MT for 30 min at 18.000 g with a Beckman Coulter Microfuge18 Centrifuge
4. Discard the supernatant and carefully resuspend the pellet in 100 - 200 μ l of BRB80T.

Attachment 3: Full matlab code – Correlation of curve with image

```
clc
clear all
%% Image time
disp('Select file of image sequence in .tif');
[ImageName,PathName] = uigetfile({'*.tif'});
imagefilename = fullfile(PathName,ImageName);
imageData = imread(imagefilename);
[token] = strtok(ImageName)
timeimage = str2num(token(end-5:end));
a = num2str(timeimage)
graph = str2num(a(1:2))
m = str2num(a(3:4))
s = str2num(a(5:6))
Timg = graph*60*60*1000 + m*60*1000 + s*1000
%% Force time
disp('Select file of curve in .xlsx');
[ForceName,PathName2] = uigetfile({'*.xlsx'});
forcefilename = fullfile(PathName2,ForceName);
forceData = xlsread(forcefilename);
[token2] = strtok(ForceName)
timeforce = str2num(token2(end-5:end));
b = num2str(timeforce)
h2 = str2num(b(1:2))
m2 = str2num(b(3:4))
s2 = str2num(b(5:6))
Tfrc = h2*60*60*1000 + m2*60*1000 + s2*1000

diference=Tfrc-Timg; %in ms
%% Time line
disp('We need time line from C-TRAP Viewer software, this
number insert in variable timeline in ms. ');
linetime=input('Time of one line in ms: ');
%% Graphs
time=forceData(:,1); %time in ms
force=forceData(:,13); %force from trap 2 in pN
distance=forceData(:,2); %distance between traps in um

figure('Name', 'Corelation on time in image and force
curve', 'NumberTitle', 'off');
subplot 211
gr=plot(time, force, 'r-');
set(gr,'LineSmoothing','On')
xlabel('Time [ms]')
```

```

ylabel('Force [pN]')
[x,y] = ginput(1);
hold on
plot(x,y,'b+', 'MarkerSize', 20);

timeinimage = x + diference;
imageline = timeinimage/linetime;

subplot 212
h=plot(time, distance, '-');
set(h,'LineSmoothing','On')
xlabel('Time [ms]')
ylabel('distance [um]')

figure
imshow(imageData(:,imageline-100:end,:))
hold on
[x1,y1,z1] = size(imageData)
line([100 100],[0 x1])

```


Attachment 4: Full matlab code – Correlation of image with curve

```
%% From Image to curve
clc
clear all

%% Image time
disp('Select file of image sequence in .tif');
[ImageName,PathName] = uigetfile({'*.tif'});
imagefilename = fullfile(PathName,ImageName);
imageData = imread(imagefilename);
[token] = strtok(ImageName)
timeimage = str2num(token(end-5:end));
a = num2str(timeimage)
graph = str2num(a(1:2))
m = str2num(a(3:4))
s = str2num(a(5:6))
Timg = graph*60*60*1000 + m*60*1000 + s*1000
%% Force time
disp('Select file of curve in .xlsx');
[ForceName,PathName2] = uigetfile({'*.xlsx'});
forcefilename = fullfile(PathName2,ForceName);
forceData = xlsread(forcefilename);
[token2] = strtok(ForceName)
timeforce = str2num(token2(end-5:end));
b = num2str(timeforce)
h2 = str2num(b(1:2))
m2 = str2num(b(3:4))
s2 = str2num(b(5:6))
Tfrc = h2*60*60*1000 + m2*60*1000 + s2*1000

diference=Tfrc-Timg; %in ms
%% Time line
disp('We need time line from C-TRAP Viewer software, this
number insert in variable timeline in ms. ');
linetime=input('Time of one line in ms: ');

%% Images
figure
imshow(imageData())
[x,y] = ginput(1);

timeofline=x*linetime;
timeincurve=timeofline-diference;
```

```

time=forceData(:,1); %time in ms
force=forceData(:,13); %force from trap 2 in pN
distance=forceData(:,2); %distance between traps in um

figure('Name', 'Corelation on time in image and force
curve', 'NumberTitle', 'off');
subplot 211
gr=plot(time, force, 'r-');
set(gr,'LineSmoothing','On')
xlabel('Time [ms]')
ylabel('Force [pN]')
hold on
plot(timeincurve,0,'b+', 'MarkerSize', 20);

subplot 212
h=plot(time, distance, '-');
set(h,'LineSmoothing','On')
xlabel('Time [ms]')
ylabel('distance [um]')

```

Attachment 5: CD

- Abstrakt_CZ.pdf
- Abstract_EN.pdf
- Key_words.pdf
- Master_thesis_Anna_Zelena.pdf
- Assignment.jpg
- Zadani.jpg